Isoprene Peroxy Radical Dynamics

Alexander P. Teng[1], John D. Crounse[1], Paul O. Wennberg[1,2]
[1]Division of Geological and Planetary Sciences, California Institute of Technology, Pasadena, California 91125, United States
[2]Division of Engineering and Applied Science, California Institute of Technology, Pasadena, California 91125, United States

Supplementary Information

Table of Contents

1. CIMS Sensitivities

For ISOPN, the sensitivity has been measured using a CIMS/TD-LIF technique described by Lee *et al*.[1] The CIMS sensitivity for ISOPOOH, HC_5, and HPALD relative to that of ISOPN is estimated using the ratio of the ion-molecule collision rates calculated according to Crounse *et al*.[2] and Paulot *et al*.[3] The sensitivity determined via the ion collision rate is multiplied by the percentage of the total ion signal from this molecule occurring at the observed *m/z*. This is not always unity due to fragmentation. This fraction is diagnosed by presence of other (fragment) ions in the chromatograms. For example, for ISOPOOH the fraction of product ions observed at the simple cluster ion (*m/z* 203) is 0.5 (see section 3a). For HPAC, HPACET, and compounds of molecular weight 116 and 132, a CIMS sensitivity of 2.0×10^{-4} normalized counts per pptv (nmcts / pptv) is used. To obtain the concentration of each molecule in the flow tube, the normalized counts (determined by dividing the signal at all masses by the reagent ion signal ($^{13}CF_3O^-$ and its cluster with H_2O and H_2O_2 (*m/z* 86 + *m/z* 104 + *m/z* 120 ≈ 70,000 ion counts per second))) is divided by the sensitivity. For example, 1 pptv of ISOPN in the instrument flow tube produces ~25 ion counts per second at *m/z* 232. In Table S1, the sensitivities are given for the simple CF_3O^- cluster (*m/z* as indicated).

Table S1 – List of compound names, measured mass to charge ratios (*m/z*), and sensitivities used in this study to convert from the signal measured at the *m/z* listed in column 2 to concentration of the compound listed in column 1. nmcts is the ion count rate at the noted *m/z* normalized by that of the reagent ions ($^{13}CF_3O^-$ and its clusters with water and hydrogen peroxide).

Compound	*m/z*	Sensitivity ($\times 10^{-4}$ nmcts pptv^{-1})
ISOPN	232	3.6
ISOPOOH	203	1.6
HPALD	201	2.8
HC_5	185	4.5
HPAC	161	2.0
HPACET	175	2.0
MW 116	201	2.0
MW 132	217	2.0

2. ISOPN (*m/z* 232)

2a. GC Elution Assignments

The ISOPN elution order is assigned using authentic standards. Synthesis, purification and identification of several ISOPN isomers (4-OH, 3-N; *E* 1-OH, 4-N; *Z* 1-OH, 4-N) are described previously.[1] Synthesis, purification and identification of the 1-OH isomers is accomplished using a new synthesis approach that will be described in a forthcoming paper. The order of the elution of the ISOPN isomers on the RTX 1701 column (Restek) follows these rules: more substituted OH groups elute earlier, more substituted ONO_2 groups elute earlier, and *Z* isomers elute before *E* isomers.

There is an unidentified peak at *m/z* 232 that elutes at the end of the separation (Figure 2 (main body), 14.5 minute elution time). This peak represents ~2% of the total ISOPN signal independent of RO_2 lifetimes. ISOPN isomer distributions analyzed at higher temperature and pressure GC programs show a much smaller signal at this peak, indicating it is thermally labile. It is possible this peak is not a nitrate functionality, but rather a nitro product of a minor branching channel in which the reactive intermediate 1-OH, 2-OONO* undergoes an isomerization (Figure S1).

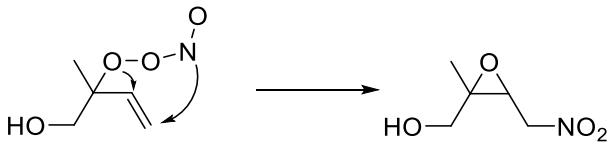

Figure S1 – Possible isomerization mechanism to form unidentified *m/z* 232 peak that elutes at 13.5 min in Figure S2 (14.5 min Figure 2, main body).

2b. Isomer Interconversion

A major challenge to the gas chromatographic analysis of ISOPN is loss and interconversion of the 1-OH, 2-N isomer to *E* 1-OH, 4-N during chromatographic separation. It also hydrolyzes quickly when water vapor is co-condensed.

2.b.i. Chromatographic separation

1-OH, 2-N ISOPN converts to the *E* 1-OH, 4-N isomer along the GC column. This produces an elevated baseline between the β and δ peaks (Figure S2). This interconversion is sensitive to temperature and pressure in the column. Elution of the 1-OH, 2-N ISOPN under higher temperatures and higher pressures increases this conversion. To accurately determine the yields of 1-OH, 2-N and *E* 1-OH, 4-N isomer ISOPN it is, therefore, necessary to minimize and account for any interconversion.

The interconversion is confirmed through three experiments. In the first, oxidation of 1-OH, 2-OOH ISOPOOH by OH with an initial concentration of 15 ppmv NO is performed. In this experiment, 1-OH, 2-N ISOPN is produced by reaction of NO with the peroxy radical formed following H-abstraction of the peroxide H. The high NO concentration results in a peroxy radical lifetime too short to allow significant decomposition of the nascent RO_2. In this experiment, GC analysis of the ISOPN shows a long, flat tailing peak after 1-OH, 2-N ISOPN which ends at the elution time of *E* 1-OH, 4-N isomer.

A second experiment to confirm the 1-OH, 2-N ISOPN interconversion during the GC utilized a heterogeneous reaction where 1-OH, 2-OOH ISOPOOH is trapped on the column, and gas-phase HONO (few hundred ppbv in air) is passed over the trapped peroxide. The HONO converts the 1-OH, 2-OOH to 1-OH, 2-N ISOPN. The chromatogram shows a similar long tail that ends at the elution time of the *E* 1-OH, 4-N ISOPN is observed.

The third test comes from a GC analysis after an ozone oxidation experiment of ISOPN isomers in which δ isomers are preferentially reacted away (the δ isomers' ozone rate constants are two orders of magnitude larger than that of the β isomers), leaving only 1-OH, 2-N and 4-OH, 3-N.[1] These chromatograms contain elevated baselines. A control analysis where only the 4-OH, 3-N isomer is analyzed by gas chromatography shows no elevated baseline.

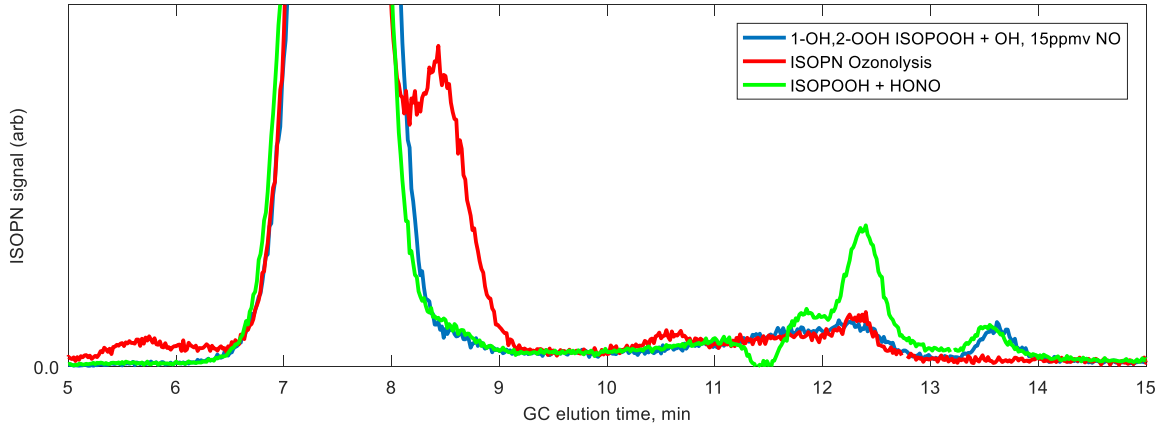

Figure S2 – Chromatogram of m/z 232 (ISOPN) illustrate the slow elevated baseline resulting from conversion of the β 1-OH, 2-N to *E* 1-OH, 4-N on the column. The small dip in the green trace at 11.5 minutes is due to the large signal peak at 233 m/z that temporarily increases the baseline and artificially reduces signal to zero temporarily.

In all three experiments, the baseline increases nearly linearly until the elution time of *E* 1-OH, 4-N. For all of the experiments listed in this study, the operating conditions for the chromatography are the same, and therefore the absolute amount of conversion is a

function only of the amount of 1-OH, 2-N trapped. A correction is modeled using these three experiments.

2.b.ii. Hydrolysis

The 1-OH, 2-N isomer hydrolyzes when water vapor is co-condensed on the column. The chromatograms shown in Figure S3 are sequential samples from the same chamber experiment. Shown in blue is the chromatogram obtained when the trapping temperature is cold enough to collect H_2O. In this experiment, a significant fraction of the 1-OH, 2-N isomer is converted to the *E* 1-OH, 4-N isomer. In addition, the expected product of hydrolysis, the 1-OH, 2-OH isoprene diol, is produced. For the data shown in the main body of this study, we scrupulously avoided trapping water on the GC column.

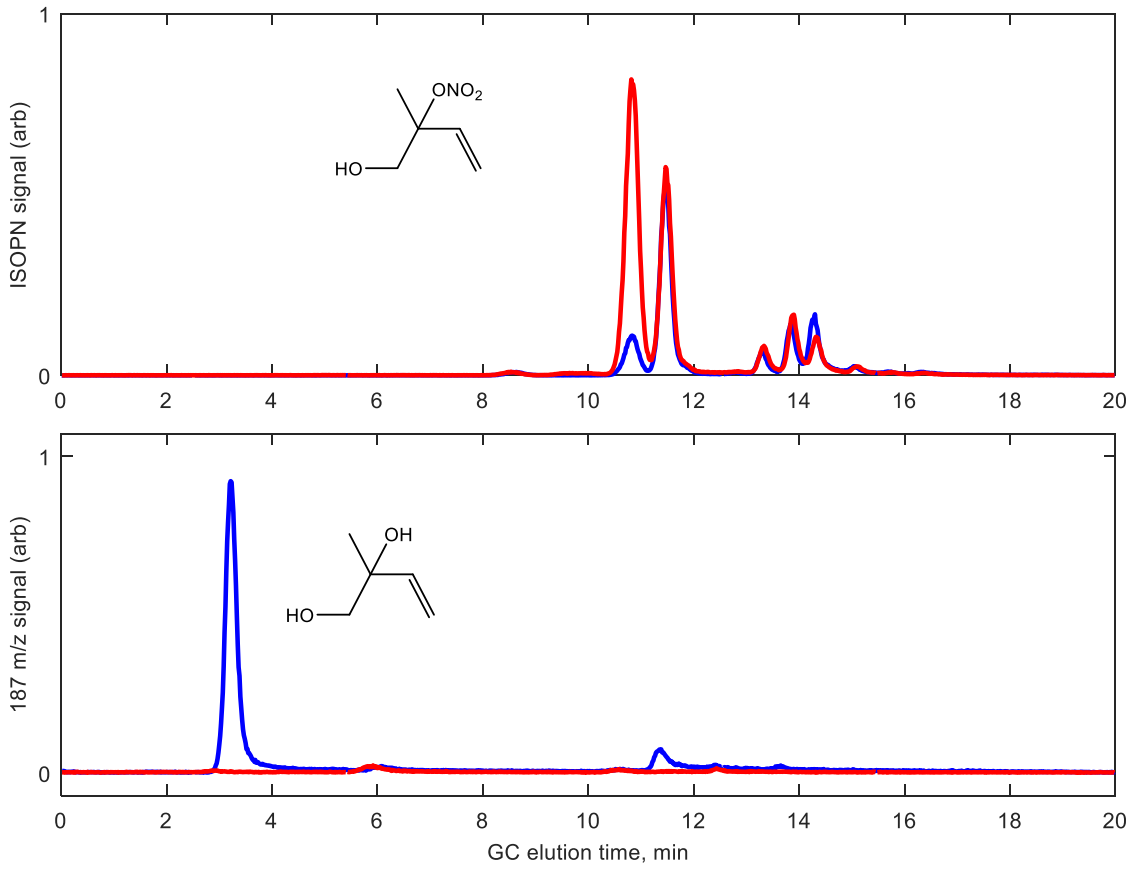

Figure S3 – Two chromatograms, taken sequentially from the same experimental chamber showing the effect of co-trapping water with ISOPN. The only difference between the operating conditions is the trap temperature (red = -20C, and blue = -45C).

2c. ISOPN formation from OH addition at C_2 and C_3

Previous studies have calculated that OH adds to isoprene at the C_2 and C_3 centers 4-7% of the time.[4–6] A synthetic standard of 2-OH, 1-N isomer (that would be produced from internal OH addition at C_2, O_2 addition to C_1, and subsequent reaction with NO), elutes before the 1-OH, 2-N isomer in the gas chromatographic analysis. The 3-OH, 4-N should, likewise, elute before the 4-OH, 3-N peak. Assigning chromatographic *m/z* 232 peaks eluting before 1-OH, 2-N (at RO_2 lifetimes < 0.01 s), to products arising from OH addition to C_2 and C_3 suggests a combined contribution of <1.5% to the signal from all hydroxy nitrates formed. Thus, there is little evidence for addition at C_2 or C_3 from measurements of the β

ISOPN isomers. It is possible, however, that the OH addition at C_2 and C_3 results in products not identified in this study due to a unimolecular chemistry occurring before O_2 addition to the OH-isoprene adduct.[7]

2d. ISOPN Yield

The isoprene nitrate yield is measured in chamber experiments in which isoprene, CH_3ONO, and NO are added to the chamber. Loss of isoprene is measured using GC-FID. Here, a PFA sampling loop on a PEEK 6-way valve connected to a 30 m PLOT-Q column in a GC-FID (Hewlett Packard 5890 series II Plus) chromatographically separates and measures isoprene from other products of the oxidation chemistry. The sampling loop is maintained at room temperature. Details of the chamber set up are described in the Methods section, and experimental conditions and results are listed in Table S2**.** The yield is corrected for loss by OH (F_corr) using the measured isomer distribution and appropriate OH rate constants (Table S3).

The reported yield is corrected to 297 K using the measured temperature increase due to the heating by the UV lamps as described in Teng *et al*.[8] The sensitivity of ISOPN isomers for CF_3O^- are determined from the same experimental setup for isoprene nitrates as described in Teng *et al*.[8] The sensitivity for all ISOPN isomers is within +-7% of the mean.

Table S2 – Experimental conditions and resulting yields for yield of ISOPN from isoprene + OH in the presence of air and NO at 297 K and 993 hPa. The calculated yield is higher by F_corr than the ratio of ISOPN measured / Isoprene loss due to photoxidation of the ISOPNs.

Exp	$[Isoprene]_o$ (ppbv)	$[NO]_o$ (ppbv)	[Isoprene] lost (ppbv)	[ISOPN] measured (ppbv)	F_corr	ISOPN Yield (%)
1	181	535	49	7.1	1.08	16 ± 3
2	24.0	490	4.1	0.5	1.04	13 ± 2
3	227	612	63	7.3	1.08	12 ± 2
4	171	504	21	2.7	1.03	14 ± 2
5	180	623	23	3.0	1.03	13 ± 2
6	199	550	43	4.2	1.05	10 ± 2
					Average:	**13 ± 2**

Table S3 – Isomer distributions and OH rate constants used to correct yield calculations. Rate constants for 4-OH, 3-N, *Z* 1-OH, 4-N, and *E* 1-OH, 4-N are taken from Lee *et al*.[1] The rate constant for the 1-OH, 2-N, *Z* 4-OH, 1-N and *E* 4-OH, 1-N were determined as part of this study, with estimated uncertainties of ±30%.

Isomer	Isomer Distribution	k_{OH} (cm^3 $molec^{-1}$ s^{-1})
1-OH, 2-N	0.50	3.0×10^{-11}
4-OH, 3-N	0.26	4.2×10^{-11}
Z 4-OH, 1-N	0.06	8×10^{-11}
E 4-OH, 1-N	0.05	8×10^{-11}
Z 1-OH, 4-N	0.04	11×10^{-11}
E 1-OH, 4-N	0.09	11×10^{-11}

A set of experiments was conducted to evaluate whether the hydroxy nitrate yield varies between isomers. A constant ratio of isoprene and 1-hexene, or isoprene and methylpropene is oxidized at two different levels of initial NO concentration. A FEP pillow bag (0.2 m^3) is filled by flowing N_2 over liquid isoprene, and then a liquid standard of 1-hexene. For methyl propene, a glass bulb of desired pressure (20 hPa) was transferred to the pillow bag. In each case, the pillow bag concentration is then checked by FT-IR, and two evacuated bulbs are filled to the desired pressure (~900 hPa). The two bulbs are used in back-to-back oxidation experiments at differing NO concentrations. The experimental conditions for both experiments are as follows: ~120 ppbv isoprene, ~140 ppbv 1-hexene, ~80 ppbv CH_3ONO. For the high NO experiment, 620 ppbv NO is added to the chamber. For

the lower NO experiment, 13 ppbv NO is added to the chamber. The extent of the reaction is terminated with <10% isoprene oxidized to minimize secondary OH losses.

The ratio of the hydroxy nitrate signals after oxidation period (Figure S4), indicate the ratio of ISOPN to 1-hexene-derived hydroxy nitrate (1-hexane HN) formed remains constant despite the difference in the ISOPN distribution (Figure S5). Given the precision of the results, however, we cannot rule out a ~10% difference in the average yields of the δ and β ISOPN isomers.

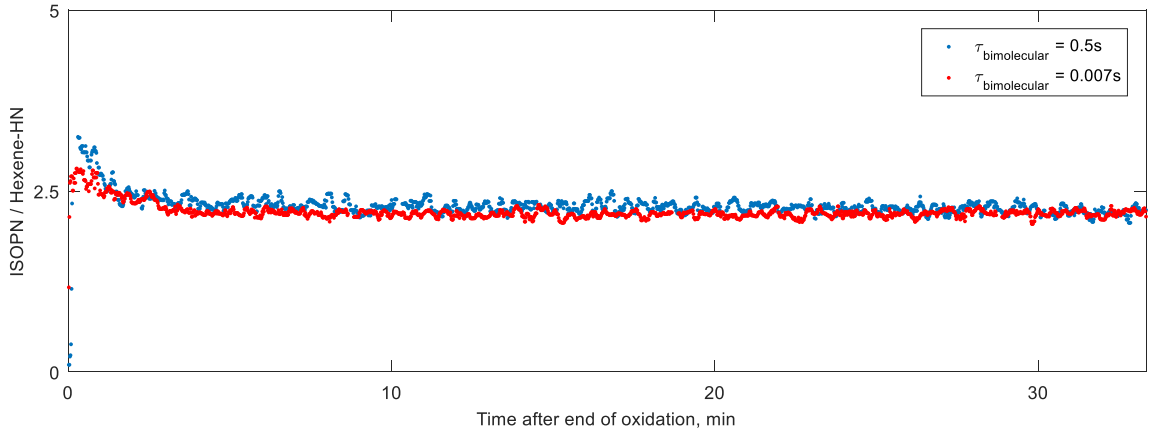

Figure S4 – The ratio of signals for *m/z* 232 (ISOPN) to *m/z* 248 (1-hexene derived hydroxy nitrate) produced during isoprene and 1-hexene + OH oxidation experiments at two different RO_2 lifetimes. The relative yields of ISOPN to 1-hexene HN do not change significantly over experiments with different RO_2 lifetimes.

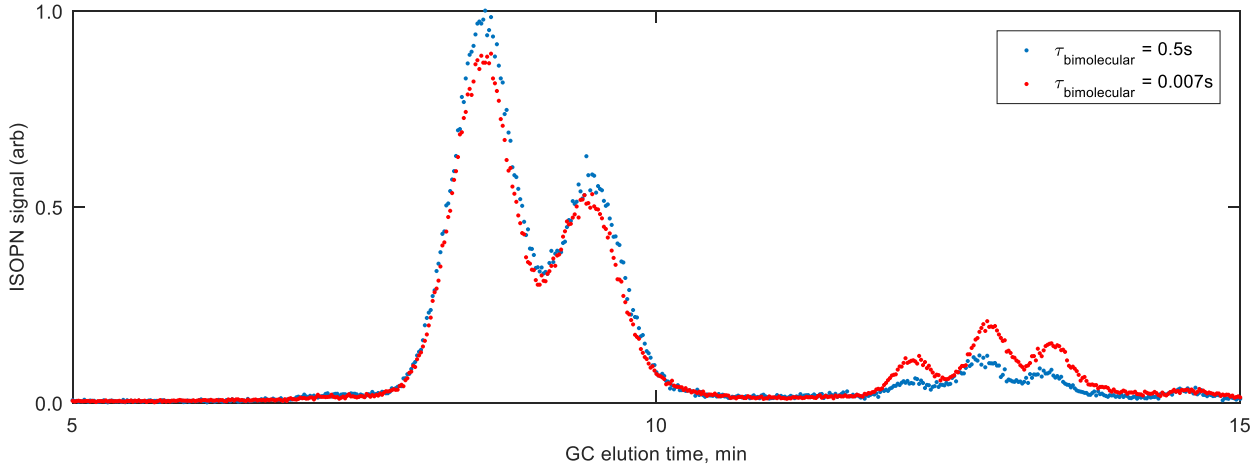

Figure S5 – GC chromatograms for *m/z* 232 (ISOPN) for the two experiments of differing bimolecular RO_2 lifetimes shown in Figure S4. Signals are normalized to the integral of the peak areas.

2e. Implied Methacrolein and Methyl Vinyl Ketone yields

The varying distribution of peroxy radicals shown in Table 2 (main body) will map into peroxy radical lifetime dependent yields for methacrolein and methyl vinyl ketone produced via reaction with NO. Accounting for the 13% yield of hydroxy nitrates, the expected yields of MVK and MACR should be 87% of the fractional abundance of the 1-OH, 2-O_2 and 4-OH, 3-O_2 isomers, respectively. The previously reported yields of methyl vinyl ketone and methacrolein at very short RO_2 lifetimes (Table S4) can be compared with our estimate for the yields of 43% and 23%, respectively, in the kinetic limit. The yields are expected to increase as the β fraction increases and then fall as H-shift chemistry becomes important. The yields reported by Spregnether *et al*.[9] agree most closely with the measured kinetic limit distribution. In the equilibrium regime, Liu *et al*.[10] report MVK and MACR yields higher than other studies, albeit statistically indistinguishable from the Spregnether study. For their conditions ($\tau_{bimolecular}$=5 s), simulations using the data presented in this study would suggest yields of 53 and 27%. Further study of the methacrolein and methyl vinyl ketone yields from the $ISOPO_2$ + NO channel at atmospherically relevant lifetimes is warranted.

Table S4 – The reported yields of methyl vinyl ketone and methacrolein from isoprene oxidation by OH from reaction of the peroxy radicals with NO (previous studies). The total β RO_2 fraction is calculated from the measured yields. The bimolecular lifetime is calculated from the reported NO concentration. For those cases where NO concentration is only reported at the start of an experiment, the bimolecular lifetime is calculated from the initial value.

Citation	MVK yield (%)	MACR yield (%)	Implied β RO_2 Fraction (%)	$\tau_{[NO]}$, s
Tuazon and Atkinson[11]	29 ± 7 33± 7[a]	21 ± 5 24± 5[a]	57 65	$6x10^{-4}$
Paulson *et al.*[12]	35.5 ± 4	25 ± 3	70	$7x10^{-4}$
Miyoshi *et al.*[13]	32 ± 5	22 ± 2	62	$\sim 6x10^{-4}$
Ruppert *et al.*[14]	31 ± 3	20 ± 2	59	$2x10^{-3}$
Sprengnether *et al.*[9]	44 ± 6	28 ± 4	83	$\sim 1.5x10^{-4}$
Karl *et al.* [15]	41±3	27 ± 3[b]	78	8-20[d]
Galloway *et al.*[16]	30.4±1.3	22.0±0.6	60	$\sim 1x10^{-2}$
Liu *et al.*[10]	44.5±5.5[c]	31.8±4.2[c]	88	5

[a] corrected for $O(^3P)$ reaction as communicated to Paulson (1992).

[b] result influenced by H-shift isomerization.

[c] assumes that 93% of the peroxy radicals react with NO.

[d] HO_2 likely contributes to this chemistry, however no measurements were made of the HO_2 concentrations.

3. ISOPOOH (*m/z* 203)

3a. GC elution assignments

Peak assignments for β ISOPOOH isomers (1-OH, 2-OOH and 4-OH, 3-OOH) are based on authentic standard synthesis (Figure S6).[17,18] No evidence of internal OH addition products is present in the *m/z* 203 chromatograms. There is a group of small peaks eluting after the β ISOPOOH isomers, tentatively identified as the δ ISOPOOH isomers. GC analysis of synthesized standard *Z* 4-OH, 1-OOH elutes within the group of peaks tentatively identified as the δ ISOPOOH isomers, but with a transmission of only ~50%. It is likely that the other δ isomers have similarly low transmission.

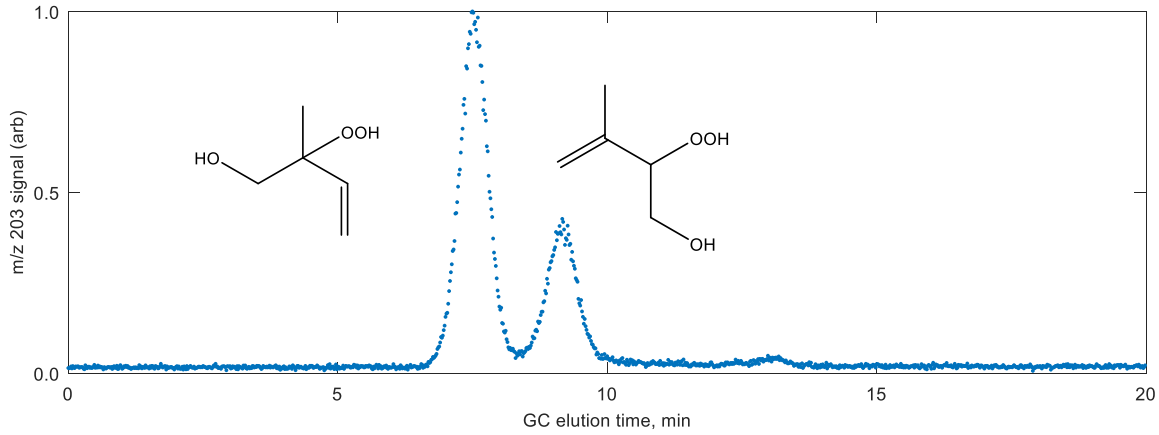

Figure S6 – Chromatogram for *m/z* 203 (ISOPOOH). δ ISOPOOH isomers (between 11 and 15 minutes) do not have 100% transmission through the GC column.

4. HPALD and other compounds (*m/z* 201)

4a. GC Peak assignments

Four main peaks are observed at *m/z* 201, corresponding to the mass of a CF_3O^- cluster ion with a neutral species of mass 116 AMU (Figure S7). MS/MS on the bulk *m/z* 201 signal yields an *m/z* 63 fragment ion with similar yield to that observed from ISOPOOH•CF_3O^- ions[2]. The +1 isotope signal observed at *m/z* 202 (arising primarily from ^{13}C) indicates the isomers observed at *m/z* 201 are composed primarily of 5 carbon compounds. The relative yield (compared to ISOPOOH and ISOPN products) of all four *m/z* 201 peaks increases as the bimolecular lifetime increases. The latter two *m/z* 201 peaks elute at temperatures in excess of the HC_5 compounds, as would be expected for the δ hydroperoxy aldehydes, and are assigned as such. Specific identification of the two latter peaks is based on their relative amounts. The HPALD derived from the 4-OH $ISOPO_2$ unimolecular channel is formed at a faster bulk rate than the 1-OH $ISOPO_2$ unimolecular channel (main body, Figure 4). However, as discussed in the main text, the yields of HPALDs from both unimolecular channels are uncertain. Nevertheless, the later eluting peak is assigned to arise from the HPALD derived from the 4-OH system and the second to

last peak is assigned to the HPALD derived from the 1-OH system, as the reverse assignment would require very disparate HPALD yields between the two systems, and this is deemed unlikely, consistent with that found for HC_5.

4b. Identity of early eluting compounds

The identities of the first two peaks observed in the *m/z* 201 chromatogram are unknown. They comprise approximately 30% of the total *m/z* 201 signal at all RO_2 lifetimes. At higher temperatures, the second peak grows larger than the first, consistent with assignment to the unimolecular channel in the 1-OH peroxy radical system.

It is unlikely these are heterogeneously produced cyclic peroxy hemiacetal rearrangement products of the HPALDs, as their concentration does not increase significantly for several hours over which GC analyses are conducted after minute-long oxidation experiments. These peaks are also not formed in the GC from the major HPALD peaks, as these compounds did not reappear in an experiment in which only later eluting HPALD peaks are cold trapped, evaporated back into a pillow bag, and re-analyzed by GC.

Because the identity of the compounds giving rise to the two early-eluting *m/z* 201 peaks is unknown, we cannot estimate the CIMS sensitivity. For this analysis, we've assumed a generic sensitivity for the early eluting *m/z* 201 peaks as listed in Table S1. It is unlikely that the sensitivity is more than a factor of two higher as the dipole moment would have to substantially exceed that of all similar molecules; a lower sensitivity cannot, however, be ruled out.

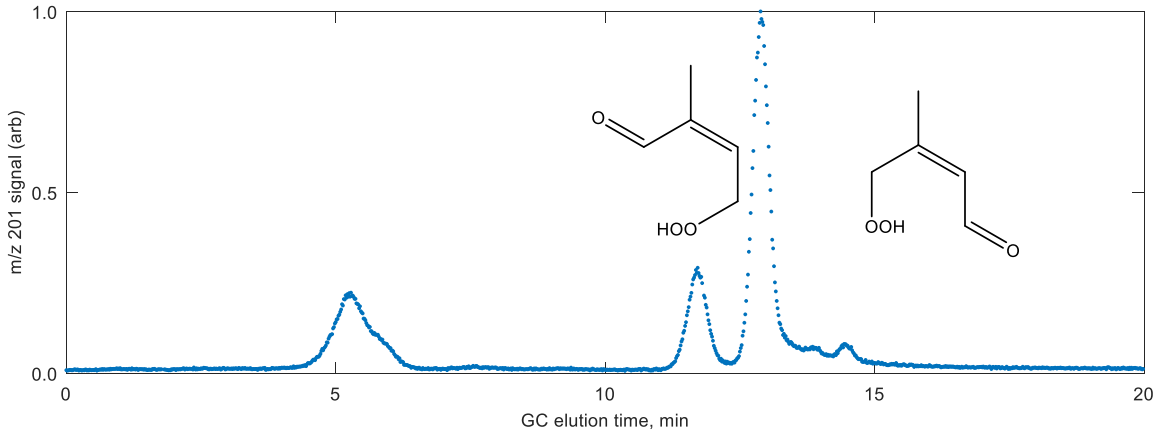

Figure S7 – Chromatogram for *m/z* 201 (HPALDs) and two other unidentified compounds are separated.

5. HC_5 (*m/z* 185)

5a. GC Peak Assignments for C_5 Hydroxy Carbonyls (HC_5, *m/z* 185)

There are only two major peaks observed in the chromatogram of the C_5 hydroxy carbonyls (HC_5, *m/z* 185, Figure S8). The identification of the elution order relies on OH oxidation experiments of 1-OH, 2-OOH and 4-OH, 3-OOH where OH abstracts the peroxide hydrogen to form either the 1-OH or 4-OH peroxy radical systems. These peroxy radicals decompose and reform producing the δ isomers. In the experiment oxidizing 1-OH, 2-OOH we observe only the first HC_5 peak; the second peak is produced in the oxidation of 4-OH, 3-OOH. This finding gives further confidence in our assignments for the HPALDs elution order.

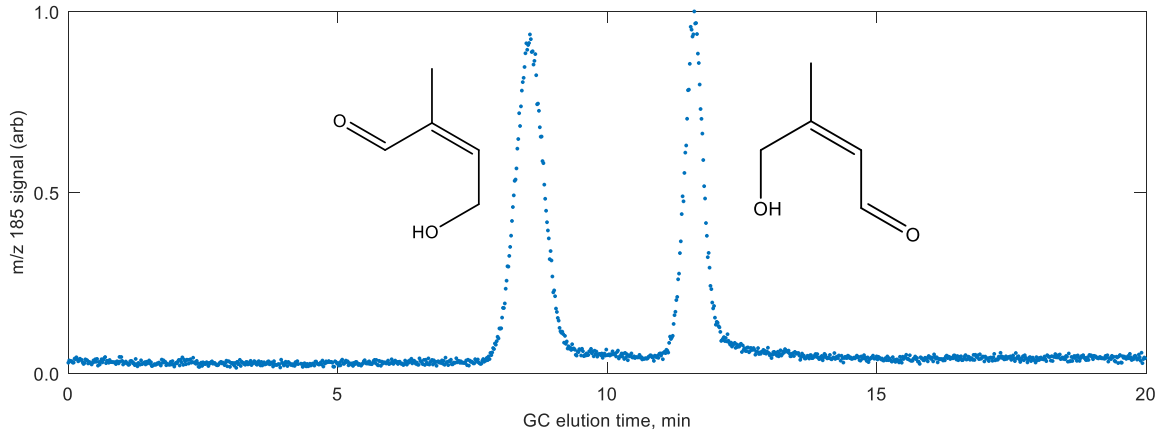

Figure S8 – Chromatogram for *m/z* 185 (HC_5) which separates the two isomers, one from the 1-OH and 4-OH system.

5b. HC_5 Yields and schemes

H-shift chemistry following reaction of the δ peroxy radicals with NO (Scheme 1, main text) gives rise to allylic radicals similar to those that yield the HPALDs. Theoretical calculations have shown that the *E* δ and *Z* δ hydroxy alkoxy radicals interconvert rapidly through an epoxide intermediate[19]. Because the rate of H-shift from the hydrogen α to the OH group in the *Z* δ isomer is much faster than conversion of the *E* δ alkoxy to HC_5 via reaction with O_2, Peeters *et al.*[19] suggested that only the *Z* δ isomers of HC_5 will form. The HC_5 chromatograms indicate that this is the case: there are only two isomers of HC_5 one each from the 1-OH and 4-OH systems. Thus, the entire pool of δ alkoxy radicals will produce the dihydroxy allylic radicals.

The chemistry following H-shift to the δ alkoxy radical (produced via reaction of the δ peroxy radical with NO) mimics that following H-shift to *Z* δ peroxy radical. As with the allylic radicals formed following H-shift RO_2 chemistry, there are two positions for O_2 addition. Addition of O_2 α to the OH group will yield HC_5. The ratio of [HC_5] to [δ ISOPN] is consistent with an HC_5 yield of 45% ±10% in both 1-OH and 4-OH systems.

As suggested by Peeters *et al.*[20], O_2 addition at either C_3 (for the 1-OH system) or C_2 (for the 4-OH system) can be followed by rapid H-shift from the enol hydroxy group from the conformer that allows this shift (Figure S9; S10). The final products when NO is very high are hydroxy acetone, glyoxal, methyl glyoxal, and glycolaldehyde – all of which are observed to form with relatively high yields.[3,16]

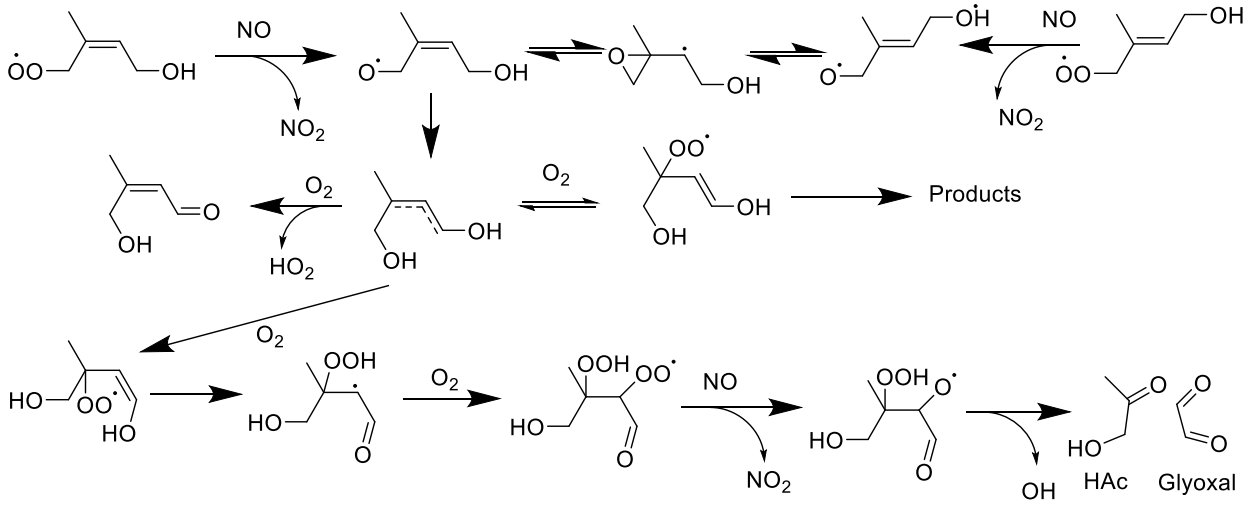

Figure S9 – Mechanism to form HC_5, hydroxy acetone (HAC) and glyoxal from the 4-OH system.

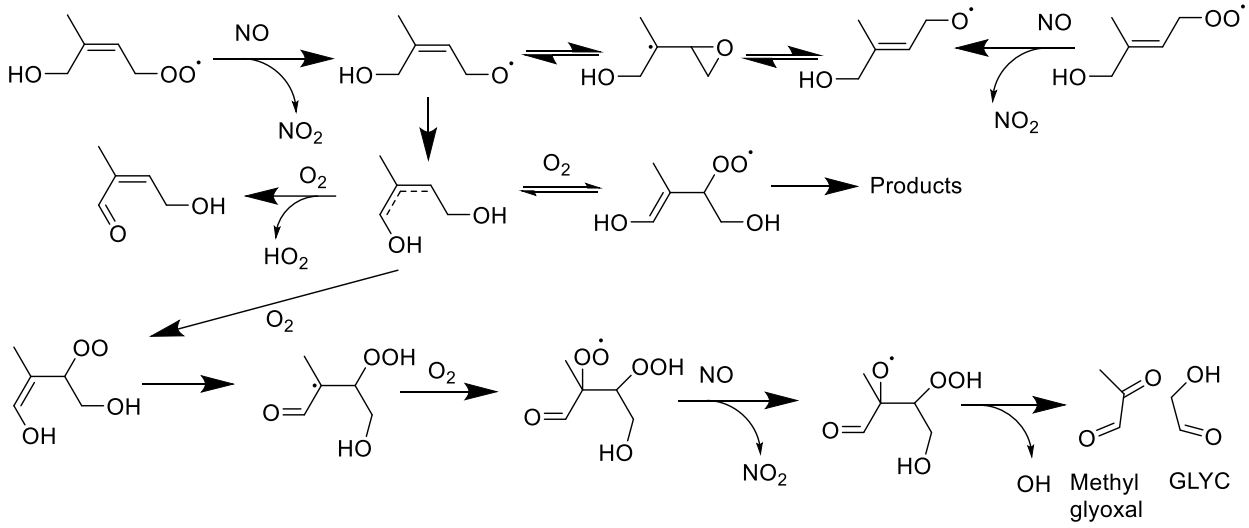

Figure S10 – Mechanism to form HC_5, methylglyoxal and glycolaldehyde (GLYC) from the 1-OH system.

6. Unimolecular H-shift of the *Z*-δ Peroxy Radicals

Following H-shift from the *Z*-δ peroxy radicals, HPALDs are formed from the hydroperoxy hydroxy allylic radical reacting with O_2 at C_1 (1-OH system) or C_4 (4-OH system). As with HC_5, however, the yield is not unity. Some of the additional products have been previously identified (hydroperoxy acetaldehyde, hydroperoxy acetone).[2] Several additional (yet unknown) products are observed here: a molecular weight 132 compound and two additional compounds of molecular weight 116 (same as HPALD) discussed in section 4b. It is unclear how these compounds form.

Proposed pathways to form HPALD compounds are shown below (Figures S11 and S12). Relative to the OH addition, O_2 addition can occur at the α position, which will eliminate HO_2 forming HPALDs. Oxygen addition at the γ position will produce two isomers, one in which the enolic hydrogen is *cis* to the peroxy radical, and another in which it is *trans*. With no obvious unimolecular chemistry, the *trans* peroxy radicals may dissociate within the lifetime of bimolecular chemistry. For the *cis* peroxy radical, the enolic H-shift is calculated to be very fast ($\sim 10^6$ s^{-1}) outrunning any other chemistry[20,21]. This produces an alkyl radical to which oxygen can add. The resulting peroxy radical will undergo rapid H-shifts with the other peroxides[22], with the fastest exit channel likely being a unimolecular H-shift from the aldehydic hydrogen. This can either result in prompt decomposition to yield CO, OH, and a dihydroperoxy carbonyl, or another oxygen can add, again yielding multiple peroxy radicals from rapid H-shift between the peroxides. The hydrogen α to the primary peroxide or the secondary peroxide are the only two available unimolecular exit channels, and are likely fast, yielding a highly substituted and oxygenated peracid.

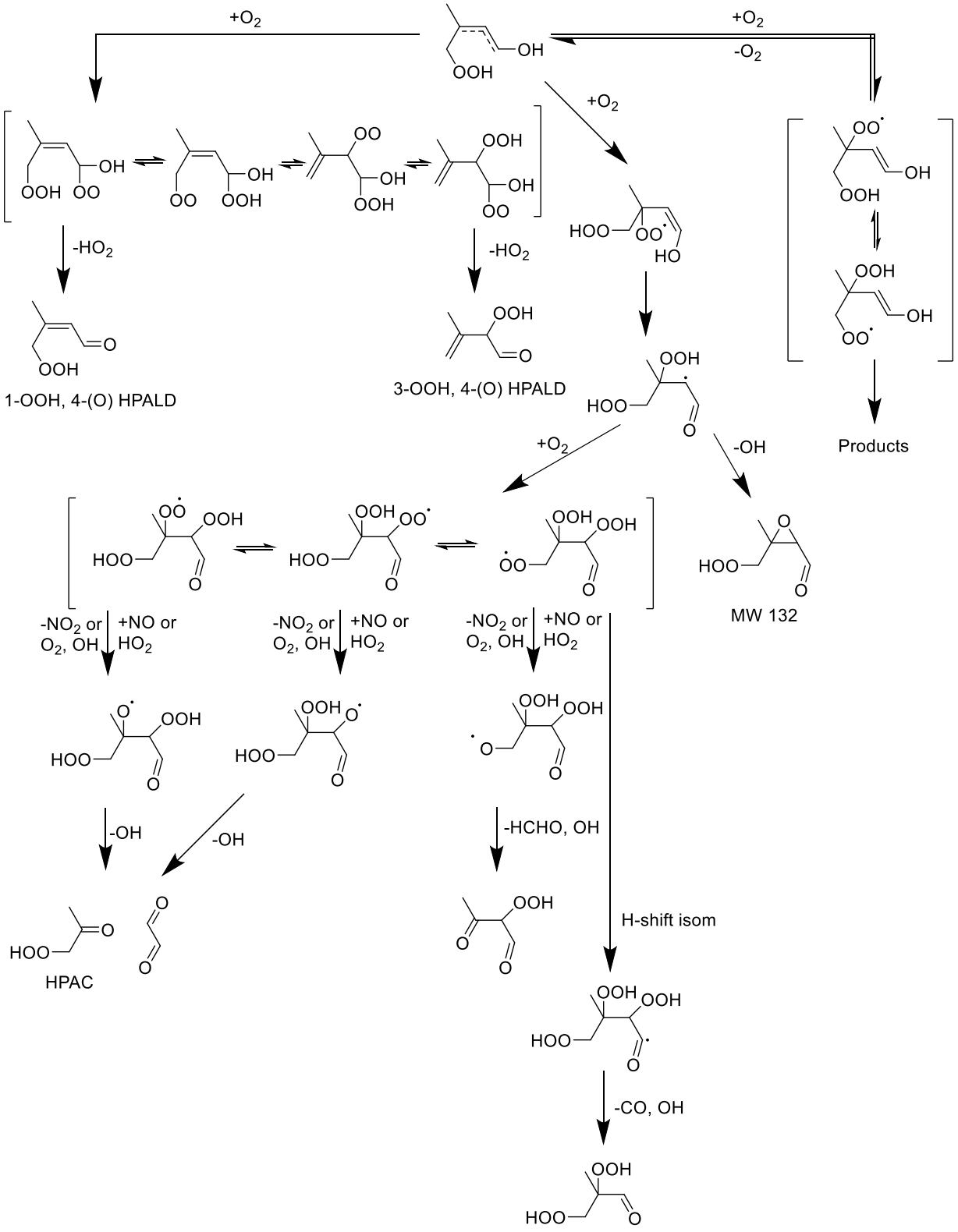

Figure S11 – Chemistry following H-shift chemistry in the 4-OH peroxy radical system. Calculations suggest that the H-shifts leading to the β peroxy carbonyls (shown on the left) are much slower than HO_2 elimination. The C_4 dihydroxy peroxy carbonyl compound shown at the very bottom of the figure is not detected by CF_3O^-, indicating it either does not form, fragments to form indiscriminate ions, or is lost to the walls.

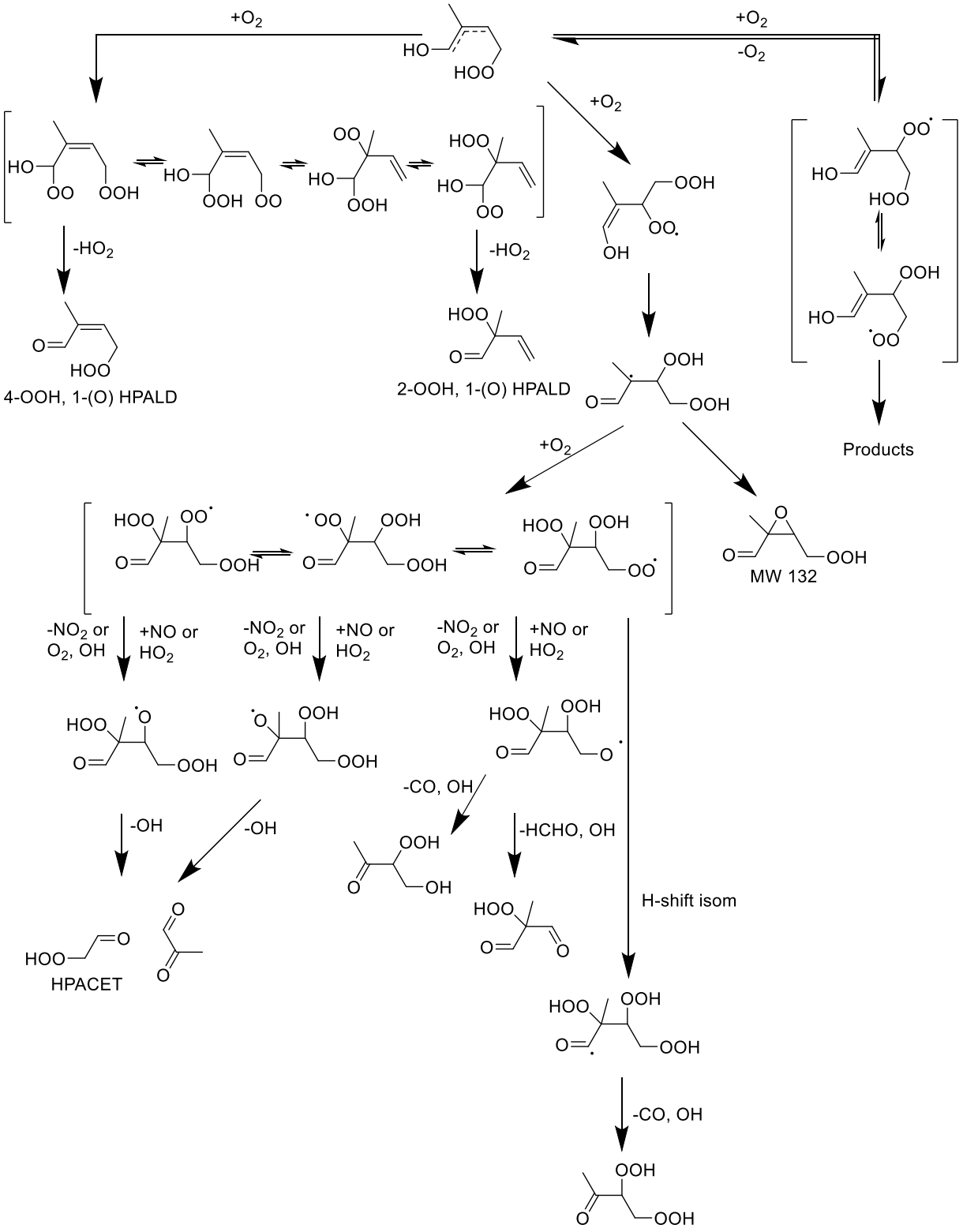

Figure S12 – Chemistry following H-shift chemistry in the 1-OH peroxy radical system. Calculations suggest that the H-shift chemistry leading to the β peroxy carbonyls (shown on the left) are much slower than HO_2 elimination. The C_4 dihydroxy peroxy carbonyl compound shown at the very bottom of the figure is not detected by CF_3O^-, indicating it either does not form, fragments to form indiscriminate ions, or is lost to the walls.

6a. Yield of HPALD

A lower bound for the fraction of the peroxy radicals undergoing H-shift isomerization following addition of OH at C_4, F_{isom4}, is approximated by 1 – 1.74*[4-OH,3-OOH]/([1-OH,2-OOH]) where 1.74 is the ratio of OH addition at C_1 relative to C_4. The ratio of unimolecular to bimolecular products can then be expressed as F_{isom} / (1 – F_{isom}). To the degree that errors in the calibration for 4-OH, 3-OOH and 1-OH, 2-OOH are correlated, this estimate for F_{isom4} is most sensitive to error in the calculated $\tau_{bimolecular}$. Most of the error in $\tau_{bimolecular}$ in turn comes from error in P_{H2O2} (e.g. the H_2O_2 sensitivity and $k_{HO2+HO2}$). The H_2O_2 sensitivity is accurate to 30% (so $k_{HO2+HO2}$ x $[HO_2]$ is accurate to 15% +uncertainty in $k_{HO2+HO2}$ [20%]). Thus, we estimate that $k_{bimolecular}$ (where $k_{bimolecular}$ is defined as 1/ $\tau_{bimolecular}$) is accurate to 35%.

With this estimate for $F_{isom,}$ we can derive the Y_{HPALD}. As shown in Figure S13, Y_{HPALD} is derived from the slope of relationship of [4-HPALD]/([ISOPN]/Y_{ISOPN} + [ISOPOOH]/$Y_{ISOPOOH}$) versus F_{isom} / (1 – F_{isom}). Accounting for the small influence of isomerization in the 1-OH system, we find that Y_{HPALD} is 25%.

From simple mass balance (adding HPALD to the other compounds assigned to H-shift RO_2 chemistry – see below), Y_{HPALD} is unlikely to be more than two times higher. From 1) HPALD calibration uncertainty and 2) uncertainty in $k_{bimolecular}$ (35%), and considering that the HC_5 yield is 45% (with its own calibration uncertainty), we suggest that Y_{HPALD} cannot be less than 15%. Thus, we estimate that the yield of HPALD is within a factor of two of 25%.

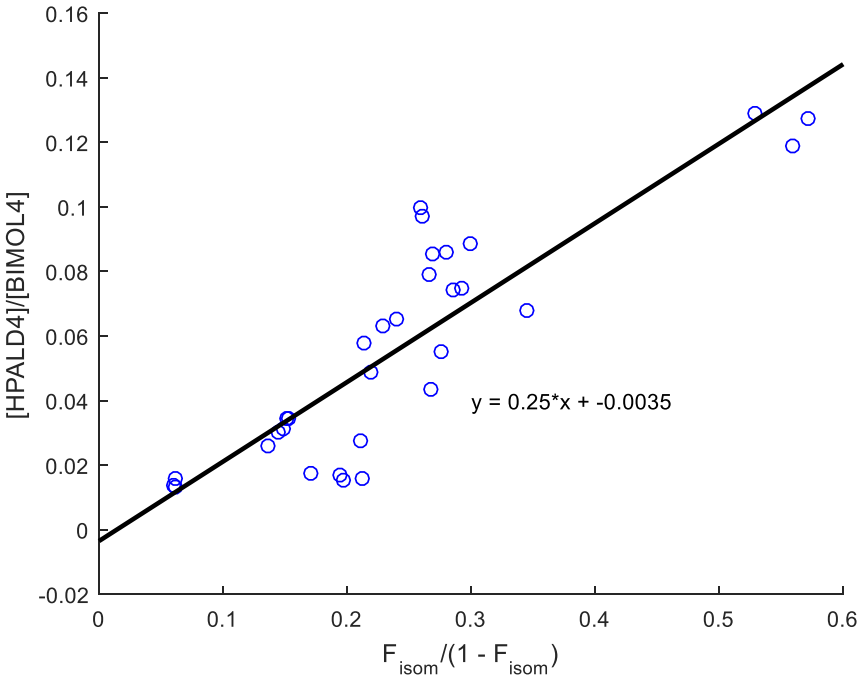

Figure S13 – F_{isom} at 297K is estimated by first calculating the total bimolecular products divided by their respective yields, i.e. [BIMOL1] = [1-OH, 2-ONO_2 ISOPN]/Y_{ISOPN} + [1-OH, 2-OOH]/$Y_{ISOPOOH}$, [BIMOL4] = [4-OH, 3-ONO_2 ISOPN]/Y_{ISOPN} + [4-OH, 3-OOH]/$Y_{ISOPOOH}$. The F_{isom} is then given as 1 – [BIMOL4]/[BIMOL1]*(0.635/0.365). Data is only plotted for $\tau_{bimolecular}$ between 1s and 40s. A least squares fit is shown above, with a slope of 0.25, the derived estimate for Y_{HPALD}.

6b. Yield of Other Products.

Yields of the observed unimolecular products are shown in Table S5. Yields for HPALDs are discussed above. Yields for compounds other than the HPALDs are derived from their production rate divided by that of HPALD using the sensitivities from Table S1 (Figure S14).

Table S5 – Yields (%) of unimolecular products at 297 K.

Compound	*Z* 1-OH, 4-O_2	*Z* 4-OH, 1-O_2
HPALD	25	25
HPACET	8.2	
HPAC	16	
MW 116	15	
MW 132	3.5	
Total	68	

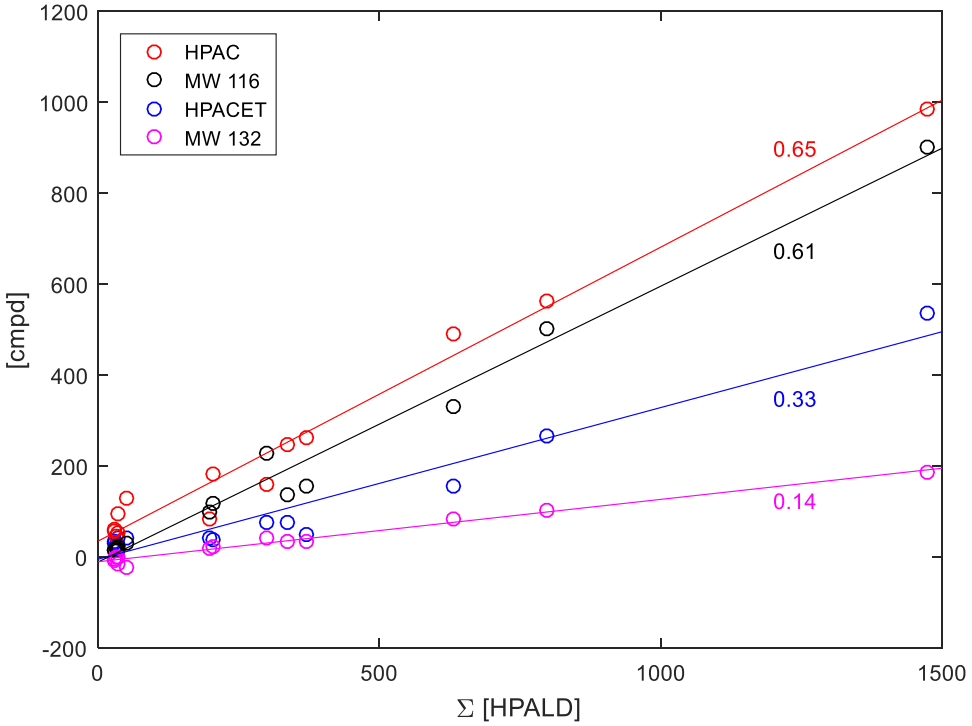

Figure S14 – Product yields at 297 K for the unimolecular channel products other than HPALDs are derived by best fits against the sum of HPALDs. The signal for each compound and the sum of all *m/z* 201 compounds are for the times when the CIMS sampled directly from the chamber (i.e. not through gas chromatograph). To derive the signal arising from the HPALDs, the total *m/z* 201 signal is multiplied by the fraction of HPALDs determined in the subsequent GC samples. Only data above $\tau_{bimolecular}$ 1 s is used in this analysis . The units for both axes are pptv.

6c. Uncertainty in the rate of peroxy radical H-shift chemistry

k_{isom4} and k_{isom1} As described in the manuscript, the rate constant of isomerization of the *Z*-δ peroxy radical isomers is estimated from the intercept (Figure 6, main body). Error in this estimate arises from several sources:

A. *Error in determining intercept*. The intercept is insensitive to $\tau_{bimolecular}$ and the assumed HPALD yield. Primarily it results from fit uncertainty (±20-40%). For the 1-OH system, for example, excluding the poorly replicated results at $\tau \approx 90$ s results in a 30% increase in the inferred intercept.
B. *Error in* $F_{Z\delta}$ *(kinetic).* Error in $F_{Z\delta}$ (kinetic) arises from the scatter in nitrate ratio determination (and number of points) in Figure 3 (main body, ±30%) and from uncertainty in nitrate yields / calibration (δ vs β yield and calibration differences, ±20%). Thus, we estimate that $F_{Z\delta}$ (kinetic) is accurate to ±40%.
C. *Error in total lifetime of the Z-δ isomers.* This is the uncertainty in identifying the inflection point in Figure 3 (main body, ±50%).

Summing these components yields an estimate of the uncertainty in k_{isom} of a factor of 3.5.

kisom x F $_{Z\delta}$ (steady-state) The product k_{isom} x F $_{Z\delta}$ (steady-state) is derived from the slope of [HPALD]/∑[bimolecular products] vs τ. Uncertainty in this estimate is very similar to that described above in 6a for F_{isom} (40%) and is limited by uncertainty in $\tau_{bimolecular}$.

F $_{Z\delta}$ (steady-state) Derived from k_{isom} and product k_{isom} x F $_{Z\delta}$ (steady-state). Uncertainty is dominated by error in k_{isom} (factor of 3.5).

F $_{Z\delta}$ (equilibrium) and ΔG (T=297) For 1-system, F $_{Z\delta}$ (steady-state) = F $_{Z\delta}$ (equilibrium) and so inherits the same uncertainty (factor of 3.5). For 4-system, error is somewhat larger as it is correlated with uncertainty in the total lifetime of the *Z* δ isomer. Uncertainty in ΔG (T=297) is propagated from uncertainty in F $_{Z\delta}$ (equilibrium).

6d. Comparison with bulk isomerization rate from Crounse, *et al.*, 2011

Several advances in our understanding of instrumental sensitivities to ISOPOOH and HPALDs have been achieved since the work of Crounse, *et al.*[2] With the addition of gas chromatography, we have found that only 50 and 85% of the ion signal arising from ISOPOOH and HPALD, respectively, are the CF_3O^- clusters (*m/z* 203 and *m/z* 201). Crounse *et al.*[2] had assumed all signal from these compounds was found at these m/z. Calibration using isomerically pure ISOPOOH, ISOPN, and IEPOX standards (St Clair *et al.*[17], Lee *et al.*[1], Bates *et al.*[23]) demonstrate that when all product ions are included, sensitivity between across these isomers nominally scales with the calculated ion-molecule collision rate (Garden *et al.*[24]). Consistent with this finding, we apply HPALD and ISOPOOH sensitivities using calculated collision rates with CF_3O^- after accounting for all observed product ions.

To derive their estimate of the bulk isomerization rate, Crounse, *et al.*[2] assumed that all the *m/z* 201 signal was from HPALD and that the yield of HPALD was 100% following H-shift. Here, using the carbon balance method, we estimate the HPALD yield to be 25% for the 4-OH system. In analogy with HC_5 yield, we assume that the HPALD yield from the 1-OH system is the same as the 4-OH system.

Together, the different sensitivity and HPALD yield explain the difference in the bulk isomerization rate calculated by Crounse, *et al.*[2] and those determined here. Applying the CF_3O^- CIMS sensitivity ratio of ISOPOOH to HPALD (Table S1) and an HPALD yield of 25% and a MW116 yield of 30% to the data presented in Crounse *et al.*, the calculated bulk RO_2 isomerization rate constant, k_{bulk_isom}(297 K), at $\tau_{biomolecular}$ = 65 s, is 0.0032 s^{-1} – identical, within uncertainties, to that determined here for the same RO_2 lifetime (Figure S15).

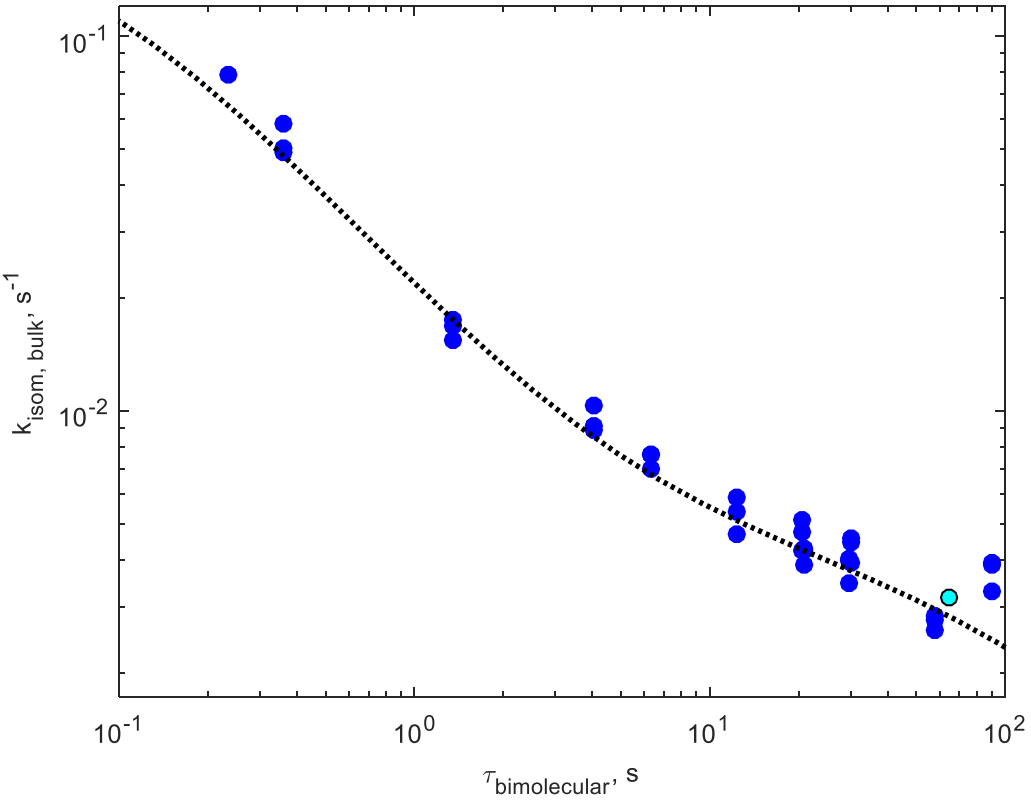

Figure S15 – $k_{isom,bulk}$ at 297 K is estimated as ([Σ HPALD]/Y_{HPALD})/({[ISOPN]/Y_{ISOPN} + [ISOPOOH]/$Y_{ISOPOOH}$}* $\tau_{bimolecular}$) (blue points). The dashed line represents the model output. A $k_{siom,bulk}$ is calculated for Crounse *et al.*, 2011 using Y_{ISOPN}, $Y_{ISOPOOH}$, Y_{HPALD} of 13%, 95%, and 25% respectively, and assuming 70% of the *m/z* 201 signal is HPALDs (teal point).

6e. Derivation of a linear approximation of products vs. τ

In the main body, in the graphical analysis shown in Fig. 6, the dependent variable contains the ratio τ / $\tau_{bimolecular}$. This factor arises from the integration of [NO] + [HO_2] dτ as described here.

Stable product formation for the bimolecular products can be expressed:

$$\frac{[ISOPN]}{Y_{ISOPN}} + \frac{[ISOPOOH]}{Y_{HPALD}} =$$

$$\int_0^{\tau} [RO_2](k_{NO+RO2}[NO] + k_{HO2+RO2}[HO_2])\, d\tau = \int_0^{\tau} \frac{[RO_2]}{\tau_{bimolec}} d\tau = \frac{\tau}{\tau_{bimolec}} [RO_2] \frac{[HPALD]}{Y_{HPALD}}$$

$$= \int_0^{\tau} [RO_2] F_{Z,\delta} k_{isom} d\tau$$

where $\tau_{bimolec} = \frac{1}{k_{NO+RO2}[NO]+k_{HO2+RO2}[HO_2]}$, and $F_{Z,\delta}$ is the fraction of Z δ peroxy radicals. We simplify the expression for the formation of HPALD by expressing the integral as two parts, the first being during the relaxation of the nascent (kinetic) Z δ peroxy radical population, and the second during the steady state $F_{Z,\delta}$:

$$\int_0^{\tau} [RO_2] F_{Z,\delta} k_{isom} d\tau = \left(F_{Z,\delta,kinetic} \frac{k_{isom}}{k_{isom} + k_{Z,\delta\rightarrow\beta}} + F_{Z,\delta,steady\ state} k_{isom} \tau \right) [RO_2]$$

where $k_{Z,\delta\rightarrow\beta}$is

We can then express the ratio of the stable products as:

$$\frac{\frac{[HPALD]}{Y_{HPALD}}}{\frac{[ISOPN]}{Y_{ISOPN}} + \frac{[ISOPOOH]}{Y_{HPALD}}} = \frac{\left(F_{Z,\delta,kinetic} \frac{k_{isom}}{k_{isom} + k_{Z,\delta\rightarrow\beta}} + F_{Z,\delta,steady\ state} k_{isom} \tau \right) [RO_2]}{\frac{\tau}{\tau_{bimolec}} [RO_2]}$$

Rearranging:

$$\frac{[Unimolecular]}{[Bimolecular]} \frac{\tau}{\tau_{bimolec}} = F_{Z,\delta,kinetic} \frac{k_{isom}}{k_{isom} + k_{Z,\delta\rightarrow\beta}} + F_{Z,\delta,steady\ state} k_{isom} \tau$$

where [Unimolecular] =$\frac{[HPALD]}{Y_{HPALD}}$ and [Bimolecular] = $\frac{[ISOPN]}{Y_{ISOPN}} + \frac{[ISOPOOH]}{Y_{HPALD}}$.

7. Experiments Constraining k_{2r}

OH oxidation experiments of 1-OH, 2-OOH ISOPOOH were performed in the presence of NO to constrain the reverse rate constant of the 1-OH, 2-OO $ISOPO_2$. A minor product of OH oxidation of 1-OH, 2-OOH ISOPOOH is the peroxy radical 1-OH, 2-OO $ISOPO_2$.[17] Synthesized standard of 1-OH, 2-OOH ISOPOOH is added to a Teflon chamber, along with CH_3ONO and varying concentrations of NO. Approximately 12% of the subsequent OH oxidation proceeds through abstraction of the H on the peroxide, leading to formation of 1-OH, 2-OO. Subsequent reaction with NO will then form ISOPN. At

bimolecular lifetimes in which O_2 is released and re-adds, *E* 1-OH, 4-OO and *Z* 1-OH, 4-OO will form. This leads to subsequent formation of the δ ISOPN isomers. The fraction of δ ISOPN isomers (*E + Z)* to the 1-OH, 2-N ISOPN provides an independent constraint on the O_2 loss rate constant for 1-OH, 2-OO $ISOPO_2$.

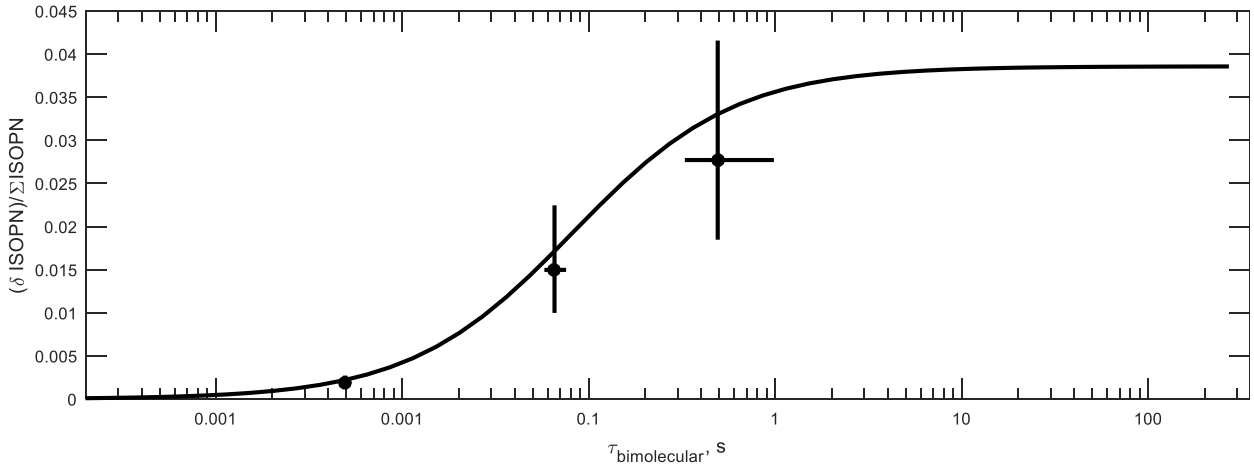

Figure S16 – The fraction of δ ISOPN formed in an experiment in which 1-OH, 2-OOH is oxidized, and ISOPN is formed upon subsequent reaction of the 1-OH, 2-OO radical with NO. The fraction of δ ISOPN formed is only possible once O_2 cleaves from 1-OH, 2-OO to form either *Z* 1-OH, 4-OO or *E* 1-OH, 4-OO. The measurement of δ ISOPN as a function of $\tau_{bimolecular}$ constrains the possible values of k_{2r}. The black line is the optimized model output of the fraction of at δ ISOPN formed 297 K for a model run in which 1-OH, 2-OOH is oxidized to form 1-OH, 2-OO.

8. Temperature dependence of the RO_2 kinetics.

To estimate the temperature dependence of the underlying kinetics, we performed a series of isoprene oxidation experiments similar to the other experiments in all respects except at elevated chamber temperature (50 C). The data from those experiments (shown in Figure S17) indicate that, as expected, the reverse O_2 rate constants increase with temperature. At elevated temperature, the transition to the kinetic limit occurs at RO_2 lifetimes <0.01 s. Unfortunately, the chromatography at $\tau_{bimolecular}$ > 10 s and T = 50 C is significantly impacted by conversion of 1-OH, 2-N from hydrolysis due to increased rate of diffusion of water into the chamber from the laboratory at the elevated temperatures.

Recommendation for the temperature dependence of the reverse O_2 rates and the 1,6 H-shifts listed in Tables S7 and S8 are derived utilizing the experimental data at 297 K and 323 K and theoretical calculations from the literature. For the loss of O_2 from the peroxy radicals, the pre-exponential values are taken from Peeters et al.[21] divided by the ratio of the calculated O_2 addition rate from Peeters et al.[21] to those listed in Table S9. The experimentally derived reverse rates shown in Table S7 are used to determine ΔH in the Van't Hoff equation. This method is sensitive to error in the O_2 addition rates and is therefore dependent on three assumptions: 1) the *cis* / *trans* OH isoprene adduct formation ratios are taken from calculations by Peeters et al.[2], 2) the absolute rate for addition of O_2 is assumed to be 2.0 x 10^{-12} cm^3 $molec^{-1}$ s^{-1}, and 3) the addition rates at the β position are equal for *cis* and *trans* OH adducts. Alteration of these assumptions would result in different temperature dependencies.

Derivation of the recommendation for the temperature dependence of the 1,6 H-shift is more complicated as we must additionally consider the role of the 1,5 H-shift of the β isomers. At room temperature, the calculated rate of the 1,5 H-shifts are very slow and do not impact the lifetime of the peroxy radicals (Crounse et al.[2]). At 323 K, however, this chemistry is calculated to significant alter the peroxy radical fate at longer RO_2 lifetimes. Therefore, the best fit 1,6 H-shift isomerization rate found from the 323 K experimental data depends on the assumed 1,5 H-shift rates. Assuming no 1,5 H-shift, the best fit values for the 1,6 H-shift are k_{isom1} = 6 s^{-1}, and k_{isom4} = 11 s^{-1}. Incorporating da Silva et al.'s[26] rates for the 1,5 H-shift reduces k_{isom1} best fit rate to 5.25 s^{-1} while using the rate from Peeters et al.[21] yields k_{isom1} = 4.2 s^{-1}. The values listed in Tables S8 assume a 1,5 H-shift rate as calculated by Peeters et al.[21]. The temperature dependence of the tunneling (C value for the

1,6 H-shifts listed in Table S8) are both assumed to be 1 x 10^8 based on Peeters et al.[21]. A and B values are then calculated from a fit between the 297 K and 323 K k_{isom} rates.

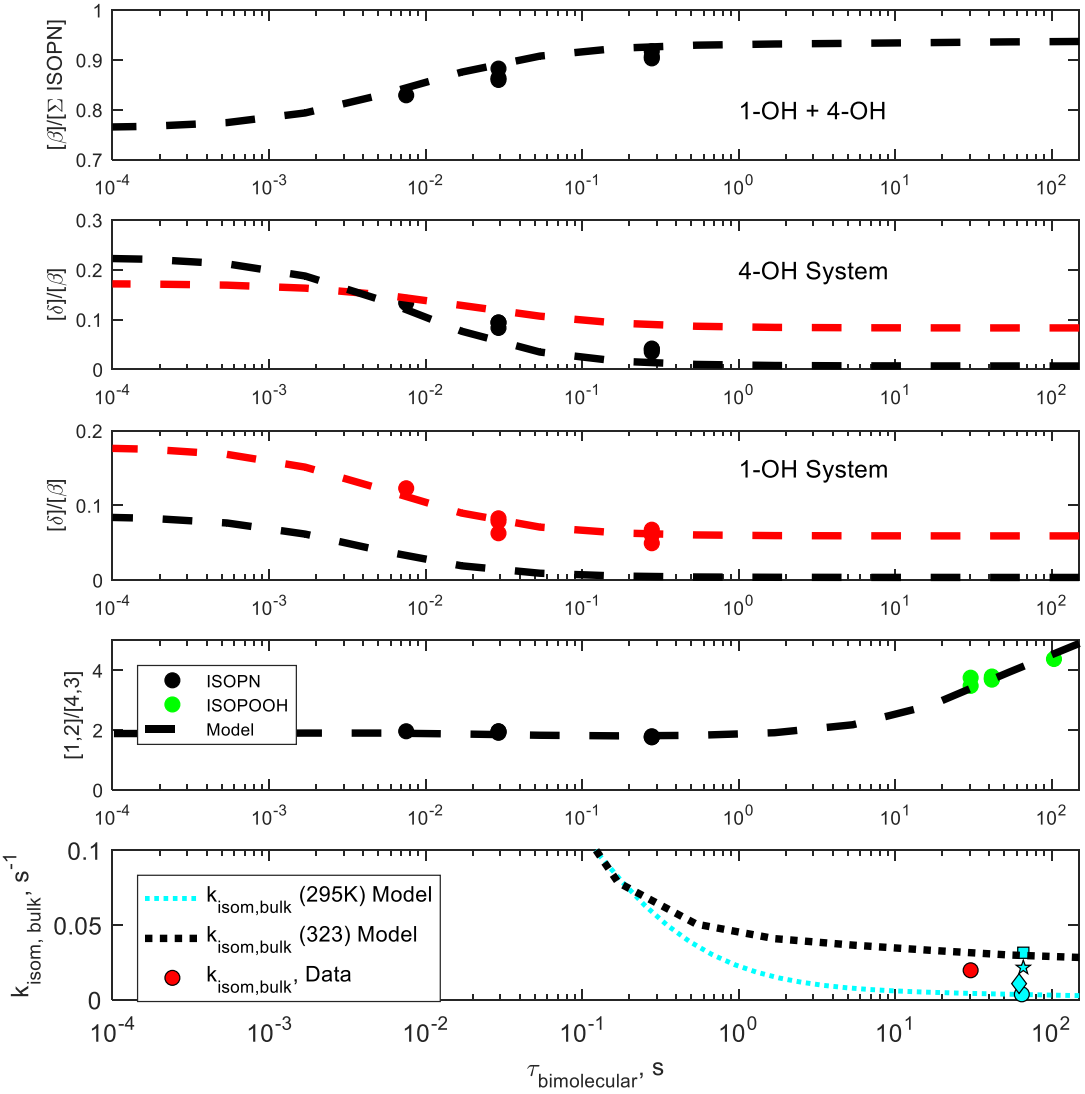

Figure S17 – A model at elevated temperature (323 K) is matched against the ISOPN isomer distribution at bimolecular lifetimes less than 1s, the ratio of ISOPOOH isomers at elevated temperatures. The bulk isomerization (filled red circle) at elevated temperatures is estimated from direct, unspeciated measurements of ISOPN (Y_{ISOPN} = 0.09 at 323 K), ISOPOOH ($Y_{ISOPOOH}$ = 0.95), and HPALDs (Y_{HPALD} = 0.25, with 0.3 of the bulk signal attributed to unknown compounds MW 116). This agrees well with the estimated bulk isomerization rate constant from Crounse *et al.*, 2011 assuming Y_{HPALD} = 0.25 is similar to the 323 K value (blue square). Measured bulk isomerization rate constants from Crounse *et al.*, 2011 at 318 K, 310 K, and 295 K are shown as a blue star, blue diamond, and blue circle, respectively.

Table S6 – Rate constants used to produce model curves shown in Figure S17 to simulate the elevated temperature experiments.

	Rate constants (323 K), s^{-1}
k_{1r}	180
k_{2r}	27
k_{3r}	5.5
k_{4r}	240
k_{5r}	48
k_{6r}	5.7
k_{7r}	2.9
k_{8r}	117
k_{isom1}	4.2
k_{isom4}	11

Table S7 – First order rate constants for the loss of O_2 from the perxoy radicals used in the model for isoprene oxidation. Temperature dependence for all rates are derived from a fit to very limited dataset at elevated temperatures, and therefore are highly uncertain.

	Rate constants (297 K), s^{-1}	A exp(-B/T)	
		A, s^{-1}	B, K
k_{1r}	16	1.83×10^{14}	8930
k_{2r}	1.6	2.22×10^{15}	10355
k_{3r}	0.29	2.24×10^{15}	10865
k_{4r}	22	1.79×10^{14}	8830
k_{5r}	3.7	2.08×10^{14}	9400
k_{6r}	0.30	2.49×10^{15}	10890
k_{7r}	0.14	2.49×10^{15}	11112
k_{8r}	10	1.75×10^{14}	9054

Table S8 – First order rate constants used in the model for isoprene oxidation for 1,6 H-shifts. Temperature dependence for all rates are derived from a fit to very limited dataset at elevated temperatures, and therefore are highly uncertain.

	Rate constants (297 K), s^{-1}	A exp (-B/T) exp (C/T^3)		
		A, s^{-1}	B, K	C, K^3
k_{isom1}	0.36	5.47×10^{15}	12200	1×10^8
k_{isom4}	3.7	2.40×10^9	7160	1×10^8

Table S9 – Implied forward rate constants calculated from the observed ISOPN isomer distribution at high levels of NO, assuming thermalized distribution ratios for isoprene-OH allylic radicals from Peeters *et al.*[5] (see Figure 1), and a total R. + O_2 rate constant of 2.0×10^{-12} cm^3 $molec^{-1}$ s^{-1} in each system.[25]

	Rate constants (cm^3 $molec^{-1}$ s^{-1})
k_{1f}	3.2×10^{-13}
k_{2f}	7.8×10^{-13}
k_{3f}	7.8×10^{-13}
k_{4f}	1.2×10^{-13}
k_{5f}	4.9×10^{-13}
k_{6f}	7.1×10^{-13}
k_{7f}	7.1×10^{-13}
k_{8f}	2.1×10^{-13}

9. Isoprene oxidation: Additional simulations

The simulations shown below (Figures S18-S25) use rate constants (Tables S7, S8, and S9) for the isoprene RO_2 system (Scheme 1) tuned to fit experimental data at 297 K. The model uses the calculated thermalized distribution of isoprene-OH allylic radicals from Peeters *et al.*[5] and an experimentally derived split of 63.5 to 36.5% between the 1-OH system and the 4-OH system.

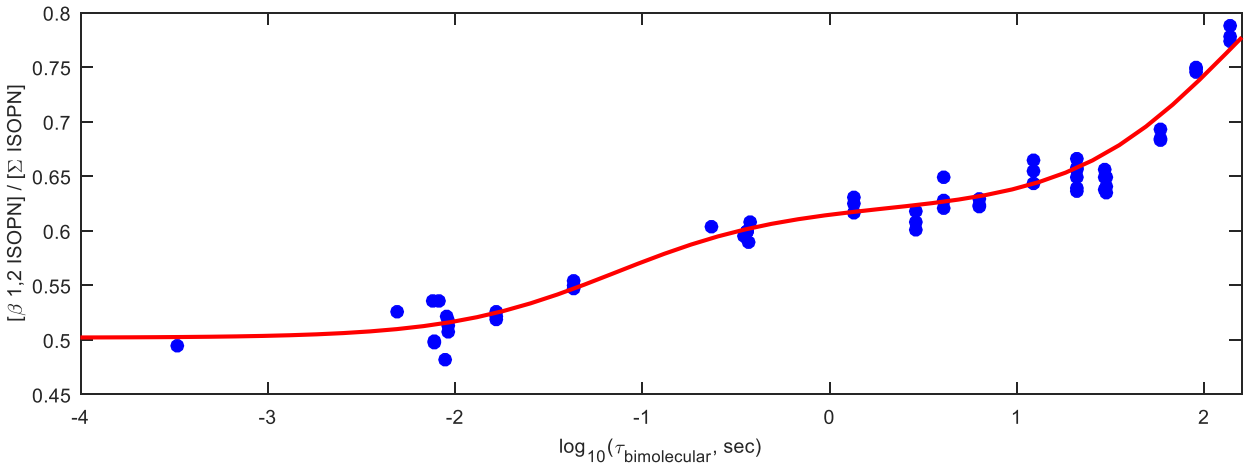

Figure S18 – Model (solid red line) simulations and experimental room temperature data (297 K) for 1-OH, 2-N distribution.

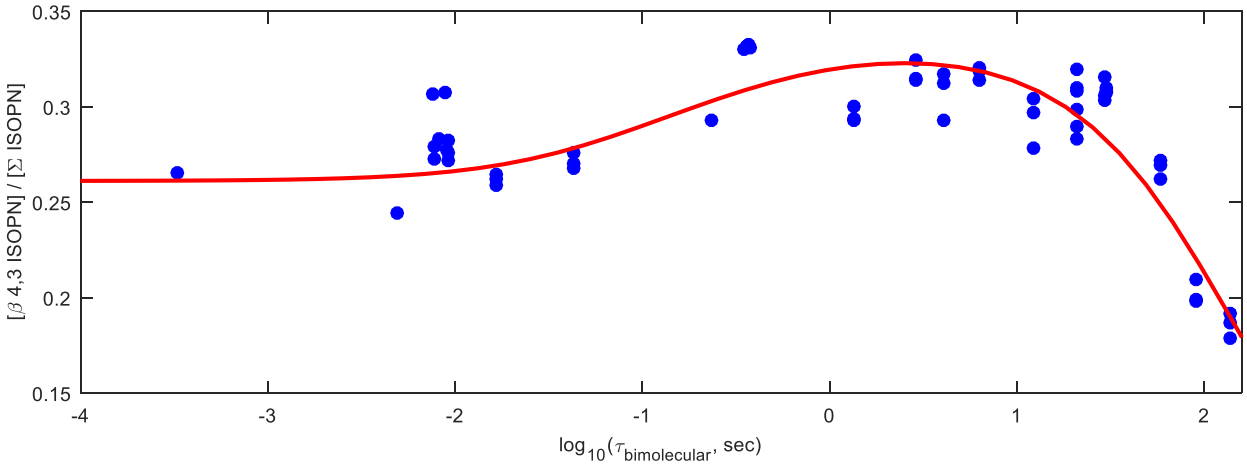

Figure S19 – Model (solid red line) simulations and experimental room temperature data (297 K) for 4-OH, 3-N distribution.

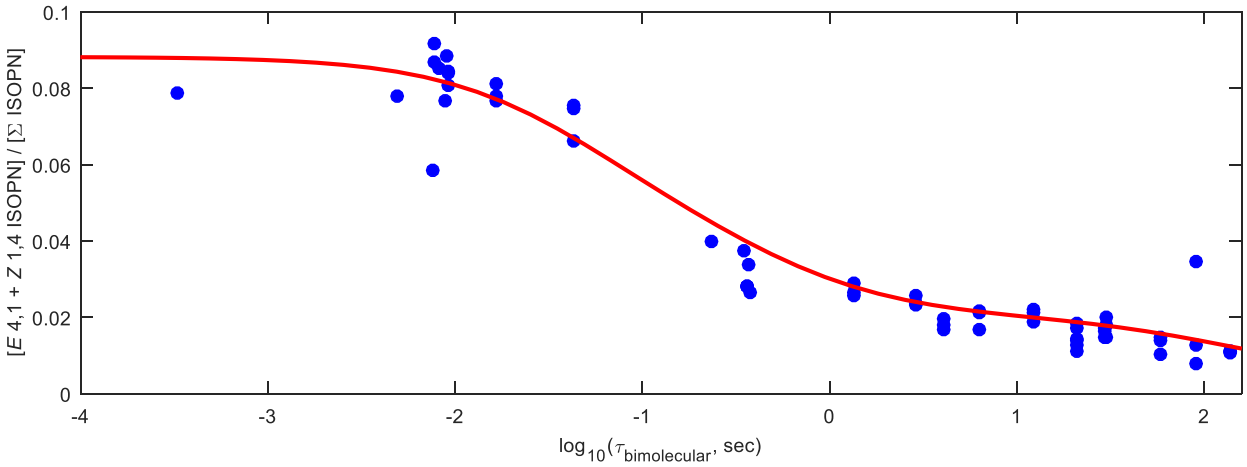

Figure S20 – Model (solid red line) simulations and experimental room temperature data (297 K) for the sum of *E* 4-OH, 1-N and Z 1-OH, 4-N distribution.

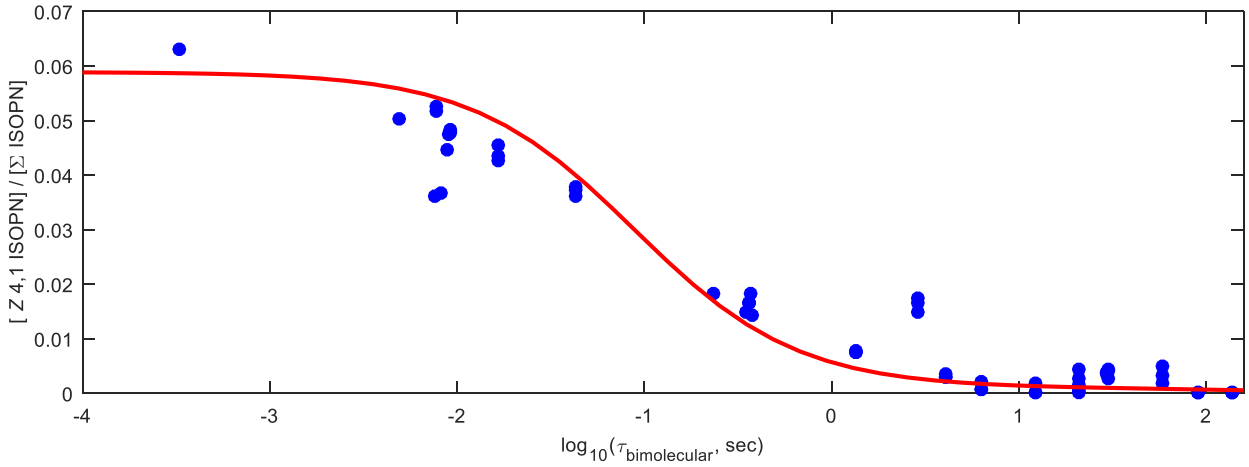

Figure S21 – Model (solid red line) simulations and experimental room temperature data (297 K) for *Z* 4-OH, 1-N distribution.

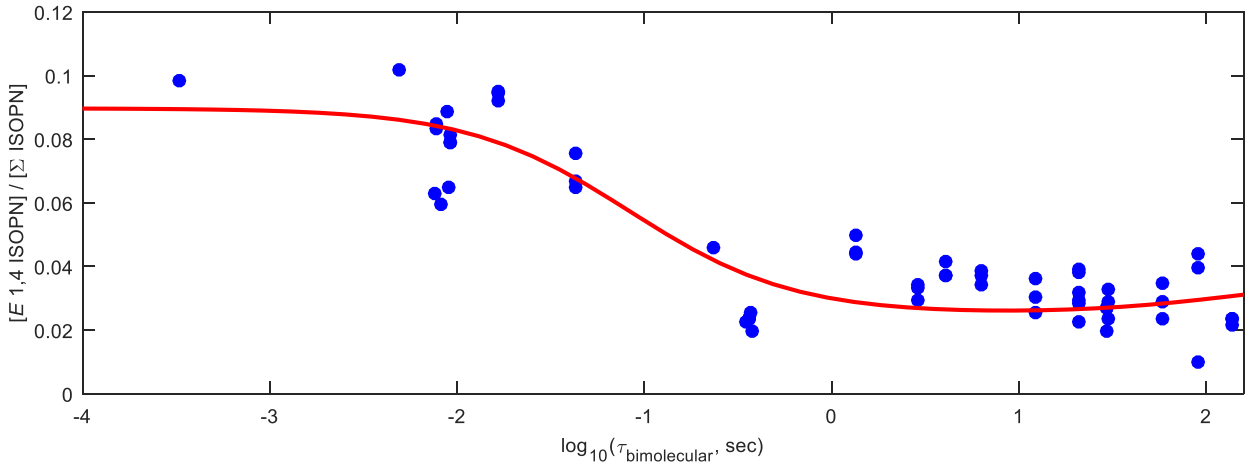

Figure S22 – Model (solid red line) simulations and experimental room temperature data (297 K) for *E* 1-OH,4-N distribution.

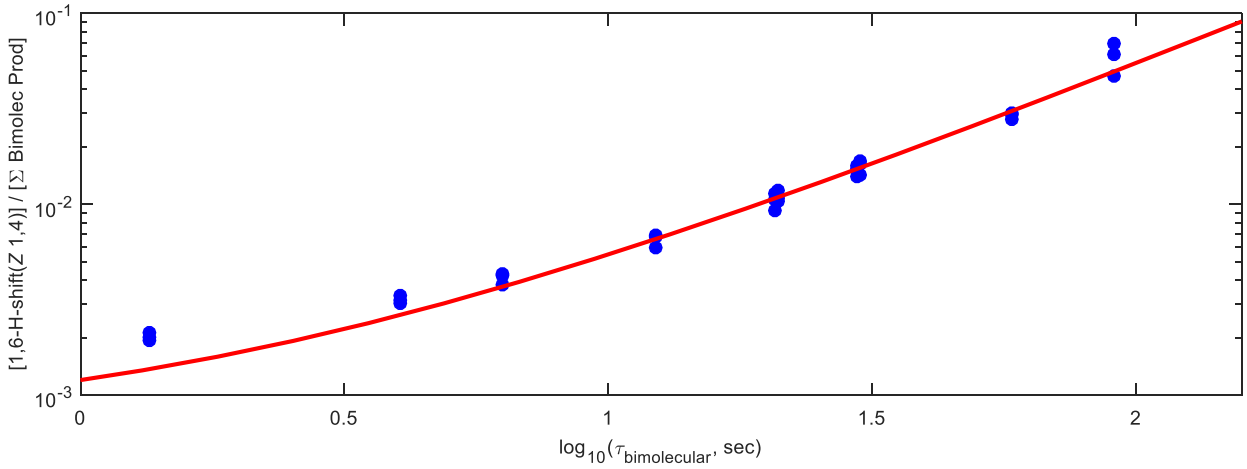

Figure S23 – Model (solid red line) simulations and experimental room temperature data (297 K) for [1-HPALD (4-OOH, 1-(O))]/Y_{HPALD} divided by [ISOPN]/Y_{ISOPN} + [ISOPOOH]/$Y_{ISOPOOH}$.

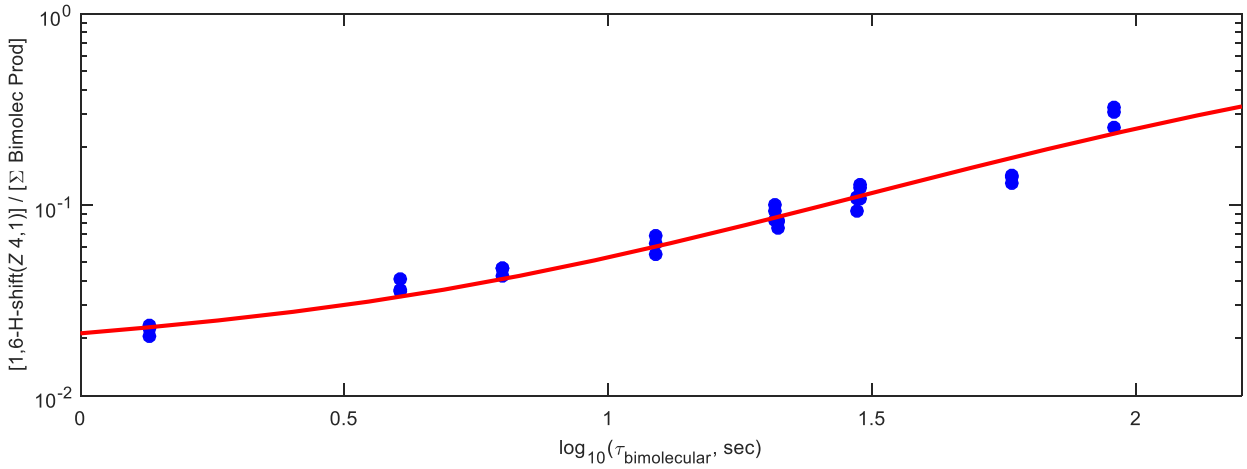

Figure S24 – Model (solid red line) simulations and experimental room temperature data (297 K) for [4-HPALD (1-OOH, 4-(O))]/Y_{HPALD} divided by [ISOPN]/Y_{ISOPN} + [ISOPOOH]/$Y_{ISOPOOH}$.

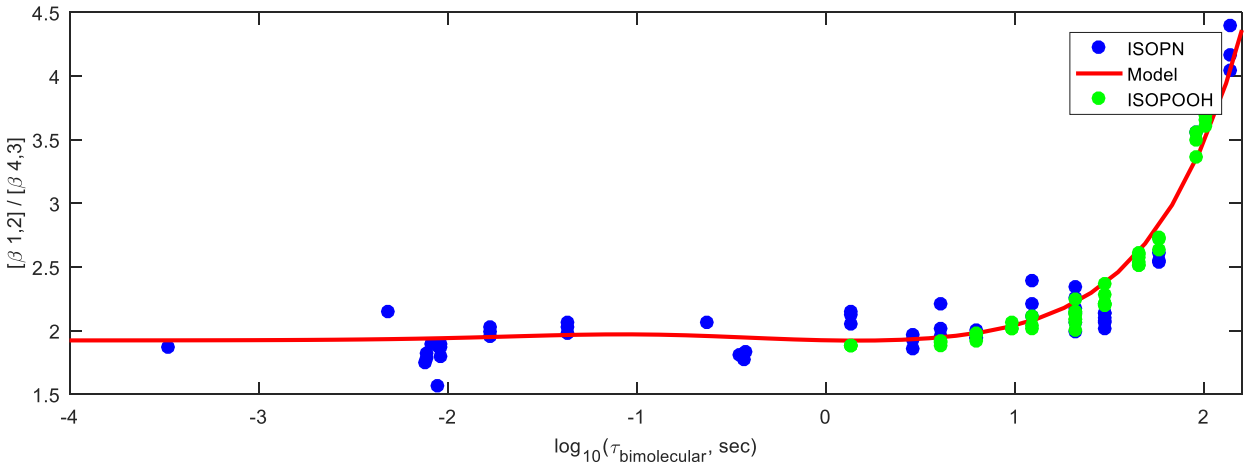

Figure S25 – Model (solid red line) simulations and experimental room temperature data (297 K) for the ratio of 1-OH, 2-X to 4-OH, 3-X. Blue and green are ISOPN and ISOPOOH measurements, respectively.

9a. Comparison with Peeters *et al.*, 2014

Using similar forward rate constants listed in Section 10, and adjusting the reverse rate constants (Table S9) to match the calculated Peeters *et al.*, 2014 ΔG values shown in Table 4 (main body) demands a much lower k_{isom} to nominally match the HPALD formation. As shown in the Figure S26, the thermochemistry from Peeters, *et al.* significantly over predicts the *Z* 4-OH, 1-OO isomer abundance. Note, the comparison using the unadjusted rates of Peeters, et al., 2014 with the data of this work is significantly less favorable. As a result of the much lower specific isomerization rate required to match HPALD at long bimolecular lifetimes, HPALD produced via isomerization of the nascent *Z*-δ population is minimal and so its production is substantially underestimated at short bimolecular lifetime.

Table S10 – Rate constants of oxygen loss calculated from Peeters *et al*., 2014 thermochemistry (Table S11), adjusted fit to observations of measured isomer distributions.

	Rate constants (297 K), s^{-1}
k_{1r}	**16**
k_{2r}	**1.4**
k_{3r}	**2**
k_{4r}	**22**
k_{5r}	**3.7**
k_{6r}	**0.08**
k_{7r}	**1.12**
k_{8r}	**10**
k_{isom1}	**0.07**
k_{isom4}	**0.5**

Table S11 – ΔG values (G_δ - G_β) calculated from the rate constants tabulated in Peeters *et al*., 2014.

δ Isomer	**ΔG (297K) (kcal/mole)***
***E* 1-OH, 4-O_2**	**2.0**
***Z* 1-OH, 4-O_2**	**2.5**
***Z* 4-OH, 1-O_2**	**2.5**
***E* 4-OH, 1-O_2**	**2.0**

*Calculated from Peeters *et al*., 2014

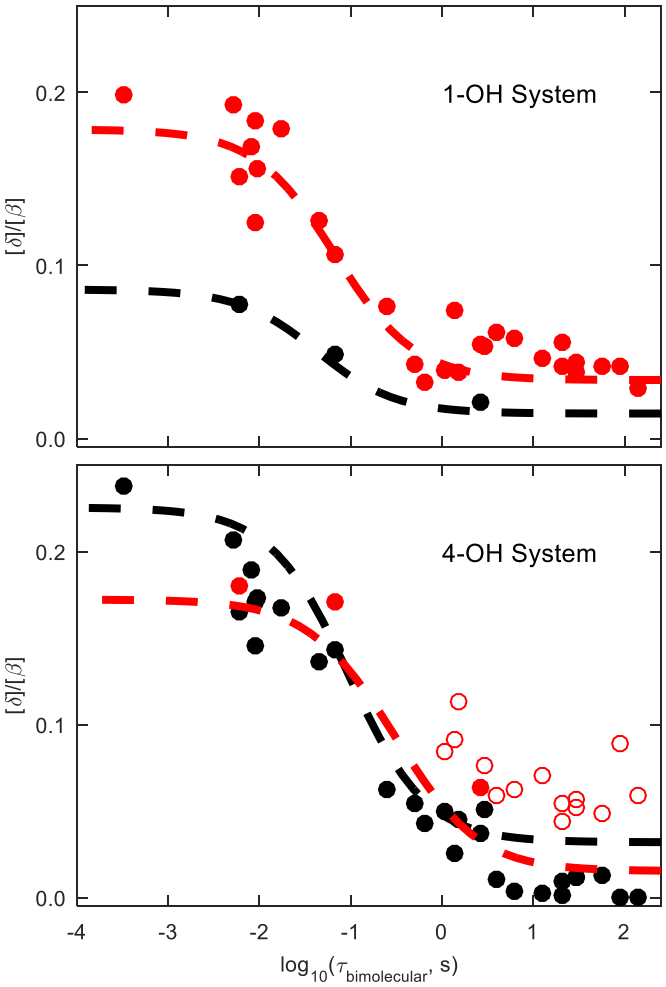

Figure S26 – Simulations using rates from Tables S9 and S10 compared to ISOPN isomer data at 297 K show that the *E* 1-OH, 4-OO data is slightly higher than predicted, *E* 4-OH, 1-OO is under predicted, and *Z* 4-OH, 1-OO is over predicted using the thermochemistry from Peeters *et al.*, 2014.

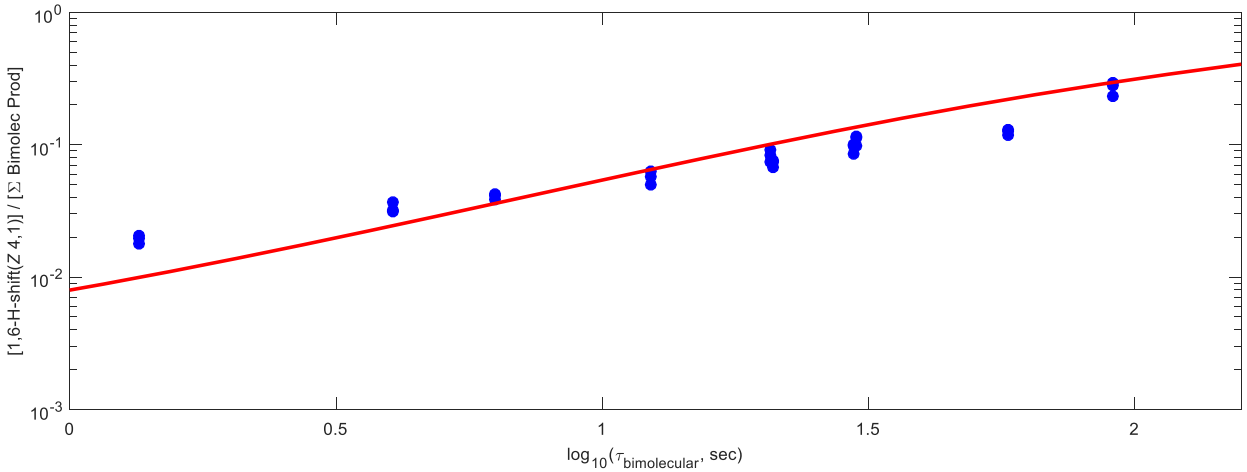

Figure S27 – Simulations using the rates in Tables S9 and S10 compared to data at 297 K show that the 4-HPALD (1-OOH, 4-(O)) is not well predicted at short bimolecular lifetimes.

10. 1,3-Butadiene and 1,3-Dimethyl-1,3-Butadiene

In the kinetic limit, the ratio of δ to β hydroxy nitrates formation decreases from 1,3 butadiene to isoprene to 2,3 dimethyl 1,3 butadiene (Figure S28). This likely reflects the decrease in electron density in the δ position of the allylic radical as compared to the β position. Following OH addition, methyl substitution β to the OH produces a tertiary radical center drawing electron density away from the δ position.

The methyl groups also affect the yield of hydroxy carbonyls upon formation of alkoxy radicals from the reaction of NO with δ peroxy radicals. For butadiene and dimethylbutadiene, we observe the formation of only one hydroxy carbonyl isomer, indicating the fast isomerization between *E* and *Z* for the alkoxy occurs in these systems as well as in isoprene. Assuming the CIMS sensitivities for the hydroxy nitrates are similar to ISOPN, we find that the nitrate yield for butadiene is 9% and for dimethylbutadiene is 10 ± 5%. Assuming the CIMS sensitivities for the δ hydroxy carbonyls is similar to HC_5, the yield of hydroxy carbonyls from reaction of NO with the δ hydroxy peroxy radicals from

butadiene is 80 ± 10%, 45 ± 10% from isoprene, and only 13 ± 8% from dimethylbutadiene. The lower yield in isoprene and dimethylbutadiene suggests that O_2 addition is substantially favored at the γ position when the allylic radical encompasses the methyl-substituted center. It is somewhat surprising, then, that the yields of HC_5 are so similar for OH addition at C_1 vs C_4 in isoprene.

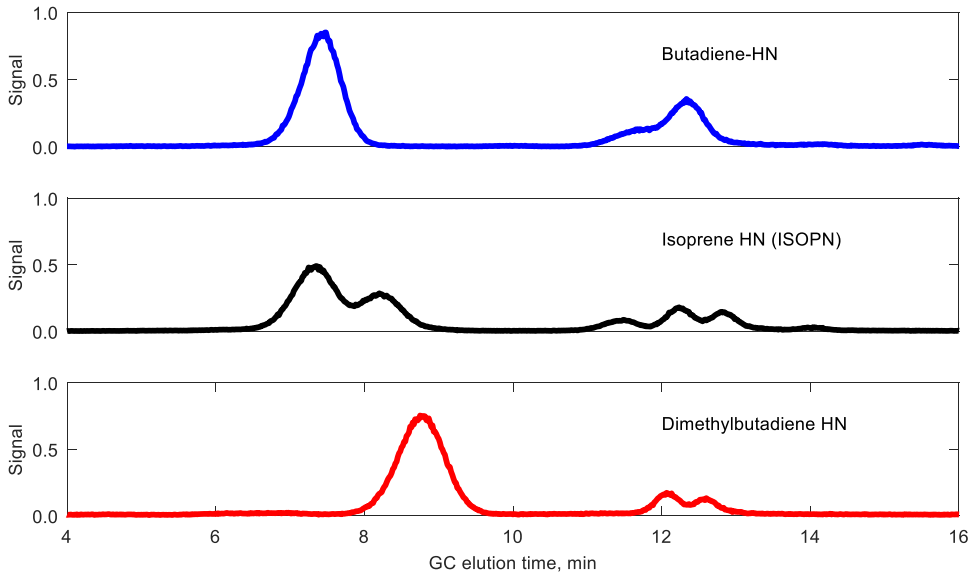

Figure S28 – Hydroxy nitrates formed from 1,3 butadiene, isoprene, and 2,3 dimethyl 1,3 butadiene (297 K) at bimolecular lifetimes less than 0.01 s. The chromatograms have been normalized to the size of the β peak(s).

11. References

(1) Lee, L.; Teng, A. P.; Wennberg, P. O.; Crounse, J. D.; Cohen, R. C. *J. Phys. Chem. A* **2014**, *118*, 1622.
(2) Crounse, J. D.; Paulot, F.; Kjaergaard, H. G.; Wennberg, P. O. *Phys. Chem. Chem. Phys.* **2011**, *13*, 13607.
(3) Paulot, F.; Crounse, J. D.; Kjaergaard, H. G.; Kroll, J. H.; Seinfeld, J. H.; Wennberg, P. O. *Atmos. Chem. Phys.* **2009**, *9*, 1479.
(4) Lei, W.; Zhang, R.; Sean McGivern, W.; Derecskei-Kovacs, A.; North, S. W. *Chem. Phys. Lett.* **2000**, *326*, 109.
(5) Peeters, J.; Nguyen, T. L.; Vereecken, L. *Phys. Chem. Chem. Phys.* **2009**, *11*, 5935.
(6) Peeters, J.; Boullart, W.; Pultau, V.; Vandenberk, S.; Vereecken, L. *J. Phys. Chem. A* **2007**, *111*, 1618.
(7) Park, J.; Jongsma, C. G.; Zhang, R.; North, S. W. *Pccp* **2003**, *5*, 3638.
(8) Teng, A. P.; Crounse, J. D.; Lee, L.; St. Clair, J. M.; Cohen, R. C.; Wennberg, P. O. *Atmos. Chem. Phys.* **2015**, *15*, 4297.
(9) Sprengnether, M.; Demerjian, K. L.; Donahue, N. M.; Anderson, J. G. *J. Geophys. Res. Atmos.* **2002**, *107*, 4268.
(10) Liu, Y. J.; Herdlinger-Blatt, I.; McKinney, K. A.; Martin, S. T. *Atmos. Chem. Phys.* **2013**, *13*, 5715.
(11) Tuazon, E. C.; Atkinson, R. *Int. J. Chem. Kinet.* **1990**, *22*, 1221.
(12) Paulson, S. E.; Flagan, R. C.; Seinfeld, J. H. *Int. J. Chem. Kinet.* **1992**, *24*, 79.
(13) Miyoshi, A.; Hatakeyama, S.; Washida, N. *J. Geophys. Res.* **1994**, *99*, 18779.
(14) Ruppert, L.; Heinz Becker, K. *Atmos. Environ.* **2000**, *34*, 1529.
(15) Karl, M.; Dorn, H. P.; Holland, F.; Koppmann, R.; Poppe, D.; Rupp, L.; Schaub, A.; Wahner, A. *J. Atmos. Chem.* **2006**, *55*, 167.
(16) Galloway, M. M.; Huisman, A. J.; Yee, L. D.; Chan, A. W. H.; Loza, C. L.; Seinfeld, J. H.; Keutsch, F. N. *Atmos. Chem. Phys.* **2011**, *11*, 10779.
(17) St. Clair, J. M.; Rivera-Rios, J. C.; Crounse, J. D.; Knap, H. C.; Bates, K. H.; Teng, A. P.; Jorgensen, S.; Kjaergaard, H. G.; Keutsch, F. N.; Wennberg, P. O. *J. Phys. Chem. A* **2016**, *120*, 1441.
(18) Rivera-Rios, J. C.; Nguyen, T. B.; Crounse, J. D.; Jud, W.; St. Clair, J. M.; Mikoviny, T.; Gilman, J. B.; Lerner, B. M.; Kaiser, J. B.; De Gouw, J.; Wisthaler, A.; Hansel, A.; Wennberg, P. O.; Seinfeld, J. H.; Keutsch, F. N. *Geophys. Res. Lett.* **2014**, *41*, 8645.
(19) Nguyen, V. S.; Peeters, J. *J. Phys. Chem. A* **2015**, *119*, 7270.
(20) Peeters, J.; Nguyen, T. L. *J. Phys. Chem. A* **2012**, *116*, 6134.
(21) Peeters, J.; Müller, J. F.; Stavrakou, T.; Nguyen, V. S. *J. Phys. Chem. A* **2014**, *118*, 8625.
(22) Jørgensen, S.; Knap, H. C.; Otkjær, R. V.; Jensen, A. M.; Kjeldsen, M. L. H.; Wennberg, P. O.; Kjaergaard, H. G. *J. Phys. Chem. A* **2016**, *120*, 266.
(23) Bates, K. H.; Crounse, J. D.; St. Clair, J. M.; Bennett, N. B.; Nguyen, T. B.; Seinfeld, J. H.; Stoltz, B. M.; Wennberg, P. O. *J. Phys. Chem. A* **2014**, *118*, 1237.
(24) Garden, A. L.; Paulot, F.; Crounse, J. D.; Maxwell-Cameron, I. J.; Wennberg, P. O.; Kjaergaard, H. G. *Chem. Phys. Lett.* **2009**, *474*, 45.
(25) Ghosh, B.; Park, J.; Anderson, K. C.; North, S. W. *Chem. Phys. Lett.* **2010**, *494*, 8.
(26) da Silva, G.; Graham, C.; Wang, Z.F.; *Environ. Sci. Technol.* **2009**, *44*, 250.